HHS Public Access

Author manuscript

Neuroimage. Author manuscript; available in PMC 2019 October 01.

Published in final edited form as:

Neuroimage. 2018 October 01; 179: 429–447. doi:10.1016/j.neuroimage.2018.06.027.

An anatomically curated fiber clustering white matter atlas for consistent white matter tract parcellation across the lifespan

Fan Zhang[a], **Ye Wu**[a], **Isaiah Norton**[a], **Laura Rigolo**[a], **Yogesh Rathi**[a], **Nikos Makris**[a], and **Lauren J. O'Donnell**[a]

[a]Harvard Medical School, Boston, USA

Abstract

This work presents an anatomically curated white matter atlas to enable consistent white matter tract parcellation across different populations. Leveraging a well-established computational pipeline for fiber clustering, we create a tract-based white matter atlas including information from 100 subjects. A novel anatomical annotation method is proposed that leverages population-based brain anatomical information and expert neuroanatomical knowledge to annotate and categorize the fiber clusters. A total of 256 white matter structures are annotated in the proposed atlas, which provides one of the most comprehensive tract-based white matter atlases covering the entire brain to date. These structures are composed of 58 deep white matter tracts including major long range association and projection tracts, commissural tracts, and tracts related to the brainstem and cerebellar connections, plus 198 short and medium range superficial fiber clusters organized into 16 categories according to the brain lobes they connect. Potential false positive connections are annotated in the atlas to enable their exclusion from analysis or visualization. In addition, the proposed atlas allows for a whole brain white matter parcellation into 800 fiber clusters to enable whole brain connectivity analyses. The atlas and related computational tools are open-source and publicly available.

We evaluate the proposed atlas using a testing dataset of 584 diffusion MRI scans from multiple independently acquired populations, across genders, the lifespan (1 day to 82 years), and different health conditions (healthy control, neuropsychiatric disorders, and brain tumor patients). Experimental results show successful white matter parcellation across subjects from different populations acquired on multiple scanners, irrespective of age, gender or disease indications. Over 99% of the fiber tracts annotated in the atlas were detected in all subjects on average. One advantage in terms of robustness is that the tract-based pipeline does not require any cortical or subcortical segmentations, which can have limited success in young children and patients with brain tumors or other structural lesions. We believe this is the first demonstration of consistent automated white matter tract parcellation across the full lifespan from birth to advanced age.

1. Introduction

Diffusion magnetic resonance imaging (dMRI) provides the only existing technique to study brain white matter structures in a non-invasive way and to map the structural connections of the living human brain (Basser et al., 1994). dMRI allows the analysis of individual white matter fiber tracts in the brain via a process called tractography (Basser et al., 2000), which has been widely used for understanding neurological development, brain function, and brain disease, as described in several reviews (Ciccarelli et al., 2008; Yamada et al., 2009; Pannek et al., 2014; Piper et al., 2014; Essayed et al., 2017). Tractography methods estimate fiber trajectories by following their probable tract orientations, enabling the measurement of microstructural white matter properties of fiber pathways (Basser et al., 2000; Mori and van Zijl, 2002; Westin et al., 2002). Performing whole brain tractography on one individual subject can generate hundreds of thousands of fibers, which are not immediately useful to clinicians or researchers. Therefore, white matter tract parcellation, i.e. dividing the massive number of tractography fibers into multiple fiber parcels (or fiber fascicles), is the first and essential step to enable tract quantification and visualization. White matter tract parcellation can enable whole brain connectivity analysis, for example via graph theory (Sporns et al., 2005; Bullmore and Sporns, 2009; Gong et al., 2009; Zalesky et al., 2012; Bastiani et al., 2012; Ingalhalikar et al., 2014; Yeh et al., 2016; Bassett and Bullmore, 2017) or fiber clustering methods (Ding et al., 2003; O'Donnell and Westin, 2007; Wassermann et al., 2010; Visser et al., 2011; Guevara et al., 2012; Jin et al., 2014; Prasad et al., 2014; Kumar et al., 2017; Garyfallidis et al., 2017; Siless et al., 2018). White matter tract parcellation is also important for identification of specific anatomical white matter tracts for clinical visualization (Nimsky et al., 2006; Golby et al., 2011; O'Donnell et al., 2017) or hypothesis-driven research (Alexander et al., 2007; Yeo et al., 2014; Wu et al., 2015; Shany et al., 2017). Though many methods exist to perform parcellation of the white matter tracts, challenges remain. Consistent automated white matter tract parcellation–across the lifespan, across different diffusion MRI acquisitions, and across healthy and patient populations–has not yet been demonstrated, to our knowledge.

In related work, most automated white matter tract parcellation methods use prior information in the form of an atlas. Gray matter atlases, e.g. those provided in Freesurfer (Fischl, 2012) or MNI–ICBM152 (Mazziotta et al., 2001), are popularly applied to parcellate white matter tracts according to their terminations in cortical and subcortical structures (Gong et al., 2009; Ingalhalikar et al., 2014; Wassermann et al., 2016). However, such methods are not yet applicable across the lifespan (Kazemi et al., 2007; Shi et al., 2011; Makropoulos et al., 2017b) and may be challenged by cortical variability (Amunts et al., 1999; Fischl et al., 1999) or prematurely terminating tractography (Yamada et al., 2009; Calabrese et al., 2014; Sotiropoulos and Zalesky, 2017). Region of interest (ROI) atlases have been proposed to define regions that are useful for selecting the trajectories of particular fiber tracts (Wakana et al., 2007; Catani and De Schotten, 2008; Lawes et al., 2008; Zhang et al., 2008; Verhoeven et al., 2010; Lebel et al., 2012; Zhang et al., 2010; Kammen et al., 2016; Wassermann et al., 2016). However, such methods can be challenged by multi-fiber tractography (which requires more ROIs to select due to its increased

sensitivity (O'Donnell et al., 2017)) and are able to parcellate a limited number of fiber tracts.

Multiple types of white matter atlas have been proposed. White matter atlases have been proposed to encode whether a particular tract is present at a particular location in the brain (voxel-based binary or probabilistic atlases (Hua et al., 2008; Hagler et al., 2009; Bazin et al., 2011; Yendiki et al., 2011; de Schotten et al., 2011; Suarez et al., 2012; Ros et al., 2013; Varentsova et al., 2014; Van Baarsen et al., 2016; Akazawa et al., 2016; Tang et al., 2018)) or to characterize tractography fibers that are representative of particular fiber tracts (tract-based atlases (Maddah et al., 2005; O'Donnell and Westin, 2007; Ziyan et al., 2009; Guevara et al., 2012; Tunç et al., 2014; Yoo et al., 2015; Guevara et al., 2017; Román et al., 2017; O'Donnell et al., 2017; Yeh et al., 2018)). These atlases are specific to the white matter, and as such may have advantages for enabling white matter parcellation.

Table 1 gives a summary of existing white matter atlases to describe the current state of the art in terms of the tracts that are defined, as well as the populations used to create and test the atlases. Most existing white matter atlases do not enable parcellation of the whole white matter, and are limited to a few fiber tracts. Initial studies have shown the potential of white/gray matter atlases to enable white matter tract parcellation across age ranges (Verhoeven et al., 2010; Lebel et al., 2012; O'Donnell et al., 2017); however the full lifespan from birth to advanced age has not yet been demonstrated. In addition, many of the atlases are not publicly available.

This work represents what we believe is the first demonstration of automated white matter tract parcellation that is consistent across the full lifespan and in a relatively large dataset of 584 diffusion MRI scans from multiple independently acquired populations (including healthy and patients with brain diseases) from different scanners. The method relies on a well-established fiber clustering pipeline from our research group (O'Donnell and Westin, 2007; O'Donnell et al., 2012), which has been successfully applied and significantly improved in our recent research studies (O'Donnell et al., 2017; Zhang et al., 2017a,b, 2018a,b; Gong et al., 2018; Sydnor et al., 2018; Wu et al., 2018). The pipeline employs groupwise fiber clustering to identify common white matter structures in a population, and it provides methods to automatically identify these structures in novel subject datasets.

A novel fiber cluster anatomical annotation method is proposed, leveraging population-based brain anatomical information and expert neuroanatomical knowledge, to annotate and categorize the fiber clusters. Each fiber cluster (a total of 800 clusters) represents an anatomical structure and its variability in 100 subjects. We note that in related work, multiple groups have previously proposed expert annotation for labeling fiber clusters (O'Donnell and Westin, 2007; Ziyan et al., 2009; Guevara et al., 2012; Tunç et al., 2014; Jin et al., 2014; Yeh et al., 2018), and many groups have studied the interactive use of fiber clustering to augment tractography visualization and annotation (O'Donnell et al., 2006; Jianu et al., 2009; Garyfallidis et al., 2012; Tax et al., 2015; Porro-Muñoz et al., 2015). A total of 256 white matter structures covering the entire brain are annotated, which generates one of the most comprehensive tract-based white matter atlases to date. These structures are composed of 58 deep white matter tracts including the major long range association and

projection tracts, the commissural tracts, and the tracts related to the brainstem and cerebellar connections, plus 198 short and medium range superficial fiber clusters organized into 16 categories according to the brain lobes they connect. Potential false positive tracts are annotated in the atlas to enable exclusion from analysis or visualization. In addition, the proposed atlas allows for a whole brain white matter parcellation into 800 fiber clusters to enable whole brain connectivity analysis. One advantage in terms of robustness of atlas-based white matter parcellation is that the tract-based pipeline does not require any cortical or subcortical segmentations, which can have limited success in young children and patients with brain tumors or other structural lesions. The pipeline and atlas (https://dmri.slicer.org/atlases) are open-source and available online, as part of the *whitematteranalysis* software[1] via the SlicerDMRI project[2] (Norton et al., 2017).

In the rest of the paper, we first describe the datasets and related preprocessing steps used in this study, followed by the generation of the proposed white matter parcellation atlas from 100 healthy adults. Then, we demonstrate our method with an application of the atlas to a total of 584 subjects (independent from the atlas population) from multiple independently acquired populations. Comprehensive quantitative and qualitative evaluations are performed to evaluate the consistency and reliability of the white matter tract parcellation.

2. Methods

Figure 1 gives an overview of the proposed work, including: (a) data-driven fiber clustering atlas generation from 100 healthy subjects (Section 2.2), (b) anatomically curated white matter atlas creation using the proposed fiber cluster anatomical annotation method (Section 2.3), (c) subject-specific whole brain white matter parcellation and (d) subject-specific anatomical tract identification by applying the proposed white matter atlas (Section 2.4).

2.1. Datasets, preprocessing and tractography

2.1.1. Datasets—In this study, we used a total of 684 subjects (100 subjects for atlas creation and 584 for experimental evaluations) across genders (253 females vs 331 males), the lifespan (neonates, children, young adults and older adults, ranging in age from 1 day to 82 years), and different health conditions (healthy control, neuropsychiatric disorders, and neurosurgical patients with brain tumors). These subjects were from multiple datasets and were scanned with different diffusion imaging protocols. Table 2 gives an overview of the demographics and the diffusion image acquisitions of the datasets under study.

1) Human Connectome Project (HCP) dataset.: The HCP dataset (Van Essen et al., 2013) (https://www.humanconnectome.org) includes high-quality neuroimaging data from *healthy young adults*. In our study, we used two data subsets from the HCP dataset. The first subset (i.e. the *HCP-atlas* dataset) consisting of 100 subjects was used for fiber clustering atlas generation and cluster anatomical annotation. The second subset (i.e. the *HCP-test* dataset) was composed of another 100 subjects (with matched ages (p-value = 0.8288 in a

[1] http://github.com/SlicerDMRI/whitematteranalysis
[2] http://dmri.slicer.org

two-tailed t-test) and the same gender distribution as the HCP-atlas subjects) for testing the white matter tract parcellation at different scales (Section 3.1).

2) Developing Human Connectome Project (dHCP) dataset.: The dHCP dataset (Makropoulos et al., 2017b) (http://www.developingconnectome.org) was used for white matter tract parcellation evaluations on data from *healthy new-born babies*. 40 individuals, ages ranging from 1 to 27 days, were studied.

3) Autism Brain Imaging Data Exchange II (ABIDE-II) dataset.: The ABIDE-II dataset (Di Martino et al., 2017) (http://fcon_1000.projects.nitrc.org/indi/abide/abide_II.html) was used for evaluations on tractography data from *children*. 70 individuals from 5 to 17 years old including 49 autism (AUT) and 21 healthy subjects were studied.

4) Consortium for Neuropsychiatric Phenomics (CNP) dataset.: The CNP dataset (Poldrack et al., 2016) (https://openfmri.org/dataset/ds000030/) was used for evaluations on data from *young adults*. The CNP dataset includes imaging data of healthy adults, as well as individuals diagnosed with neuropsychiatric disorders including schizophrenia (SZ), bipolar disorder (BD) or attention-deficit/hyperactivity disorder (ADHD). In our study, we used a population of 204 subjects.

5) Parkinson's Progression Markers Initiative (PPMI) dataset.: The PPMI dataset (Marek et al., 2011) (http://www.ppmi-info.org) was adopted for evaluations on data from *older adults*. In our study, we used 144 subjects, including Parkinson's disease (PD) patients and healthy individuals.

6) Brain Tumor Patient (BTP) dataset.: A retrospective dataset from 26 neuro-surgical patients was used for evaluations in generalizing to *brains with tumors*. Imaging data was acquired at Brigham and Women's Hospital. The usage of the data was approved by the Partners Healthcare Institutional Review Board, and informed consent was obtained from all participants prior to scanning.

2.1.2. Data preprocessing—Here, we introduce the data preprocessing steps used for each dataset. The output of the data preprocessing included a diffusion MRI scan per subject, which was well corrected to exclude any potential artifacts, e.g., from eddy current and head motion effects. In addition, a Freesurfer brain segmentation was obtained upon a successful application of the Freesurfer software. Table 2 lists the availability of Freesurfer segmentations for each dataset. The Freesurfer segmentations were used in this study for the following purposes: 1) the initial cluster annotation computation for the anatomically curated atlas creation (Section 2.3.1), 2) experimental evaluations for tract anatomical coherence (Section 2.5.3), and 3) experimental comparisons with the WMQL-based methods (Section 3.3.2). We note that for whole brain white matter parcellation and anatomical tract identification using our method, the Freesurfer segmentation results were not required. Details of the preprocessing steps for each dataset under study are included in Appendix A.

2.1.3. Multi-fiber tractography—We conducted whole brain tractography using a two-tensor unscented Kalman filter (UKF) method (Malcolm et al., 2010; Reddy and Rathi,

2016), as implemented in the ukftractography[3] package. The UKF method fits a mixture model of two tensors to the diffusion data while tracking fibers. In contrast to other methods that fit a model to the signal independently at each voxel (Qazi et al., 2009), in the UKF framework each tracking step employs prior information from the previous step to help stabilize model fitting. The two-tensor UKF model was shown to be more sensitive than standard single-tensor tractography, in particular in the presence of crossing fibers and peritumoral edema (Baumgartner et al., 2012; Chen et al., 2015, 2016; Liao et al., 2017). For each of the subjects under study, there were about 1 million fibers in the whole brain tractography. Details of the related tractography parameters are included in Appendix A. Visual and quantitative quality control of the tractography was performed using a quality control tool in the *whitematteranalysis* software. (To demonstrate the proposed parcellation method's ability to generalize to tractography data from different methods, we have included another two tractography methods, as introduced in the supplementary material.)

2.2. Whole brain fiber clustering white matter parcellation atlas learned from 100 healthy subjects

A whole brain fiber clustering atlas was generated using a well-established data-driven fiber clustering pipeline, including groupwise tractography registration (O'Donnell et al., 2012) and groupwise spectral clustering of tractography (O'Donnell and Westin, 2007; O'Donnell et al., 2017). The pipeline has been shown to have high performance in our recent research studies (O'Donnell et al., 2017; Zhang et al., 2017a,b, 2018a,b; Gong et al., 2018; Sydnor et al., 2018; Wu et al., 2018). The fiber clustering divides the whole brain tractography into multiple fiber clusters (as shown in Figure 1(a)) in a data-driven fashion according to the common white matter anatomy across multiple subjects. Details about the fiber clustering pipeline for atlas generation are included in Appendix B.

In this study, a large population of 100 HCP healthy adults (see Section 2.1.1 for demographics) was used to learn the fiber clustering atlas. 10,000 fibers were randomly sampled from each subject's full tractography for a total of 1 million fibers for the fiber clustering atlas generation. Related parameters were set to the default settings in the *whitematteranalysis* software. We generated multiple fiber clustering atlases to investigate the whole brain white matter parcellation at different scales (number of clusters, K, ranging from 200 to 4000). An atlas consisting of $K = 800$ clusters[4] was chosen (see experiments in Section 3.1 and Discussion in Section 4 supporting this choice) for anatomical curation (Section 2.3). During this stage, we also generated a population mean T1 image by transforming all subjects' T1 images into the fiber clustering atlas space according to the groupwise tractography registration. This population mean T1 image was used to assist the expert judgment when creating the anatomically curated atlas.

2.3. Anatomically curated white matter atlas creation

Given the chosen fiber clustering atlas ($K = 800$), each fiber cluster was annotated with an anatomical label (e.g. the corticospinal tract (CST)) to create an anatomically curated white

[3] https://github.com/pnlbwh/ukftractography

[4] Please see the video S1 included in the supplementary material for a visualization of each individual fiber cluster within this atlas.

matter atlas for anatomical tract identification. Each anatomical tract consists of multiple fiber clusters, where each cluster represents a white matter structure and its anatomical variability across the 100 subjects, as illustrated in Figure 1(b). A novel fiber cluster anatomical annotation method is proposed to annotate and organize the clusters, as illustrated in Figure 2, including an initial cluster annotation computation, followed by expert judgment.

2.3.1. Initial fiber cluster annotation computation—The purpose of this initial computation step is to bootstrap the expert cluster annotation with a first pass that can be performed automatically by the computer. This is crucial to enable expert annotation of such a large dataset, which is not possible in the traditional way of independently visualizing all data from each subject. (100 subjects times 800 fiber clusters gives a total of 80,000 fiber clusters that would need to be viewed.) We propose a strategy of computing a potential annotation for each cluster by leveraging all known anatomical information across all 100 HCP-atlas subjects, including subject-specific fiber clusters and cortical and subcortical segmentation information (Freesurfer segmentation (Fischl, 2012) was used). Unlike the atlas creation, which relied on a sample of fibers (10,000 fibers per subject), this step leveraged subject-specific fiber clusters that were computed from the full tractography from each of the 100 HCP-atlas subjects. This data was on the order of 1 million fibers per subject (including the 10,000 fibers in the atlas), and was clustered using the atlas (following the computations introduced in Section 2.4.1). In this way, we could use the maximal tract information from these 100 subjects for the initial fiber cluster annotation. We note that the cortical and subcortical segmentations were only used for assisting the anatomically curated atlas creation, while white matter tract parcellation for a new subject (Section 2.4.1) did not require any cortical or subcortical segmentations.

There were two initial automated fiber cluster annotation steps, as illustrated in Figure 2. First, we applied White Matter Query Language (WMQL) (Wassermann et al., 2016), which provides anatomical definitions of fiber tracts based on their intersected Freesurfer regions, to initially identify fiber clusters potentially belonging to common association, commissural and projection tracts. WMQL allows extraction of anatomical tracts based on the labeled Freesurfer regions through which the fibers pass (or do not pass), known as anatomical definitions[5]. In our study, the basic idea of this step was to use the fibers with known anatomical definitions within a cluster to compute a potential anatomical label. WMQL anatomical definitions of 45 tracts were used. Specifically, given a cluster c and an anatomical tract t, we calculated how many fibers within c met the WMQL definition of t in each HCP-atlas subject. Then, we considered that the cluster c had an initial potential label of the tract t if at least one HCP-atlas subject had fibers in c meeting the definition of t.

Second, we computed a tract anatomical profile (TAP) of each cluster, i.e. the set of segmented brain Freesurfer regions through which the cluster passed, for identifying another 13 deep white matter tracts (e.g. the cerebellar tracts) and the superficial tracts. This gave an

[5]Anatomical tract definitions in WMQL are written as queries that are established by an expert neuroanatomist (NM). A query file that defines 45 anatomical tracts can be found at https://github.com/pnlbwh/pnlutil/blob/master/pipeline/wmql-2.0.qry. We note that the queries are an updated version of those originally presented in (Wassermann et al., 2016), reflecting improvements following query testing and modification by NM and colleagues.

initial potential annotation of tracts that were not defined in WMQL. The TAP was calculated based on the 100 HCP-atlas subjects, as follows. For a cluster *c*, we first computed the set of intersected Freesurfer regions of each fiber per subject. Then, we identified the set of regions intersected by all or most fibers across all subjects to define the cluster's TAP. In our study, we included a region into a cluster's TAP if at least 40% of fibers of this cluster across the 100 subjects intersected with this region (see Appendix C for the choice of this threshold). As a result, the TAP provided population-based characteristics of the brain regions though which a cluster passed. (We note that the TAP of each cluster is provided along with the proposed atlas in the *whitematteranalysis* software.) Next, the computed TAP was used for initial cluster annotation. For example, for the potential cerebellar tracts, we identified all clusters with a TAP containing any cerebellum-related Freesurfer regions (i.e. cerebellum-white-matter and cerebellum-cortex). In addition, potential superficial fiber clusters were identified and organized into categories based on their connecting brain lobes, including within-lobe connections and connections between neighboring lobes. This gave 8 categories of superficial fiber clusters per hemisphere, for a total of 16 categories including both hemispheres.

The initially annotated tracts covered almost 90% of the 800 clusters, while the remaining were annotated as initially unclassified. Given the initial annotation output, we obtained a small number of potential candidate clusters for each tract (e.g. 17 fiber clusters potentially belonging to the CST were initially identified) for expert judgment. We note that any misidentified clusters during the initial annotation process would be corrected by the expert judgment, and any clusters that were missed (e.g. classified to another tract category) would be also corrected.

2.3.2. Expert fiber cluster annotation judgment—The purpose of this step was to perform final expert annotation of the fiber clusters by a neuroanatomist (NM), in order to produce the anatomically cu-rated white matter atlas. This step leveraged the previous initial annotation computation to make it possible for the neuroanatomist to view data from all subjects for every tract in an organized way. For each tract, groupwise data (atlas fiber clusters containing fibers from all 100 subjects) and individual subject data were viewed until a determination was made about the annotations of all clusters within the tract. For each cluster, the neuroanatomist accepted or rejected the initial annotation result, and he gave correct annotations when the initial annotations were rejected.

Specifically, for each fiber cluster, the neuroanatomist (NM) viewed the 3D tract overlaid on an anatomical T1-weighed image in the 3D Slicer software, including the following two steps. First, the atlas fiber cluster was viewed with reference to the population mean T1 image (Section 2.2) from all HCP-100 subjects. This enabled viewing of the white matter structure and its variability across all HCP-100 subjects. Then, to confirm the population-based decision, the corresponding subject-specific cluster from a randomly selected HCP-atlas subject was checked with reference to the subject's T1 image. Additional subjects were visualized as needed to clarify the decision of the cluster annotation. We note that for some clusters that were judged to clearly belong to a certain anatomical tract, we did not need to perform the second step in the individual subjects. For example, the apparent C-shaped fiber clusters connecting the temporal, parietal, and frontal lobes belonged to the arcuate

fasciculus (AF) tract. A final iteration of expert checking was conducted by viewing the whole anatomical fiber tract by combining all individual clusters together in the atlas. This step allowed identification of any clusters that were inconsistent with the others within a tract.

58 deep white matter tracts and 198 superficial fiber clusters organized into 16 categories according to their connecting brain lobes were annotated in the proposed atlas, as shown in Table 3. These tracts consisted of a total of 510 clusters (312 deep white matter clusters and 198 superficial clusters), accounting for 63.75% of all clusters in the fiber clustering atlas (K = 800). In addition, any possible false positive tracts from tractography errors were identified. For example, there were fiber clusters connecting the cerebellum and cortex in the same hemisphere, which are expected to cross the hemispheres (Schmahmann, 1996); there were partially traced corpus callosum tracts without connecting inter-hemispheric cortex (Makris et al., 1999). 18.75% of all clusters were considered to belong to the false positive category. The remaining 17.5% of clusters were annotated as unclassified.

Each annotated anatomical tract, as well as the potential false positive tracts, were organized in a 3D Slicer scene file (in medical reality modeling language (MRML), an XML format). The MRML file allows visualization of the whole anatomical tract and each individual cluster within the tract in 3D Slicer (O'Donnell et al., 2017). All MRML files are provided in the proposed anatomically curated atlas[6].

2.4. Application of fiber clustering atlas to new subjects

In this section, we introduce how to apply the obtained fiber clustering atlas along with the curated anatomical annotations to perform subject-specific whole brain white matter parcellation and anatomical tract identification for a new subject. We note that the whole brain white matter parcellation and the anatomical tract identification are computed using the subject's tractography data only, without requiring any cortical or subcortical segmentations.

2.4.1. Subject-specific whole brain white matter parcellation—Whole brain white matter parcellation of a new subject was conducted by performing a fiber clustering on the subject's tractography according to the fiber clustering atlas, which is briefly introduced as follows. First, an entropy-based tractography registration to the atlas tractography was computed to align the new tractography to the atlas space (O'Donnell et al., 2012). Then, subject-specific fiber clusters were detected using spectral embedding of the registered tractography, followed by assignment of each fiber to the closest cluster (O'Donnell and Westin, 2007). Outlier fibers were removed if their fiber affinity regarding the atlas cluster was over 2 standard deviations from the cluster's mean fiber affinity (as applied in (O'Donnell et al., 2017; Zhang et al., 2018a)). As a result, the new subject's tractography was divided into multiple fiber clusters, where each cluster corresponded to a certain atlas fiber cluster, as illustrated in Figure 1(c).

[6]Please see the video S2 included in the supplementary material for a visualization of each anatomical tract.

2.4.2. Subject-specific anatomical tract identification—Anatomical tract identification of the new subject was conducted by finding the subject-specific clusters that corresponded to the annotated atlas clusters, as shown in Figure 1(d).

2.5. Evaluation measurements

All subjects' whole brain tractography was parcellated using the proposed white matter atlas. Then, we applied the following measurements to quantitatively evaluate the white matter parcellation performance.

2.5.1. White matter parcellation generalization—White matter parcellation generalization (WMPG) was used to measure the percent of fiber clusters that could be successfully detected in an individual subject. Specifically, given a fiber clustering atlas consisting of a total of K fiber clusters, we calculated the number of clusters (NC) with at least 20 fibers in a subject s, and computed the WMPG as:

$$WMPG(s) = \frac{NC(s)}{K} \quad (1)$$

Here, we chose a threshold of 20 fibers for the WMPG computation. Many works that study the white matter connections have defined a threshold on the number of fibers to decide whether a white matter connection exists or not. For example, Brown et al. considered that two brain regions were connected if there were at least 3 fibers between them (Brown et al., 2011). In another study, thresholds from 1 to 15 fibers were optimal for different brain white matter network metrics (Drakesmith et al., 2015). In our study, we chose a relatively high threshold of 20 that is more strict to decide if a fiber cluster was successfully detected. A high WMPG value indicates a high generalization of the atlas to this subject.

2.5.2. Inter-subject parcellation variability—Inter-subject parcellation variability (ISPV) was used to evaluate if there were similar numbers of fibers in a corresponding fiber cluster across multiple subjects. For a fiber cluster c, we computed the number of fibers (NF) of this cluster for each subject, and calculated the coefficient of variation (CV) of NF across the subjects to measure the ISPV, as:

$$ISPV(c) = CV(c) = \frac{Std(NF(c))}{Mean(NF(c))} \quad (2)$$

where $Std(NF)$ and $Mean(NF)$ are the standard deviation and the mean of NF across all of the subjects. Equation 2 is the coefficient of variation of the number of fibers of a cluster across different subjects, where a low value represents a low parcellation variability and thus a high consistency across the subjects. This measure has been applied in recent studies to measure white matter parcellation consistency (Roberts et al., 2017; Zhang et al., 2017b).

2.5.3. Tract anatomical profile coherence—Tract anatomical profile coherence (TAPC) was used to investigate if the fibers within a cluster commonly passed through the

same brain anatomical regions (i.e. Freesurfer regions). To do this, we measured the overlap between each subject-specific fiber's set of intersected Freesurfer regions (i.e. TAP of the fiber) and its atlas cluster's TAP (see Section 2.3.1 for definition and Appendix C for more details, including a figure illustrating TAPC computation). The Dice score (Dice, 1945) has been widely used to evaluate the overlap between two sets (i.e. $\frac{2|A \cap B|}{|A| + |B|}$ for sets A and B) in tractography-based studies (Pecheva et al., 2017; Cousineau et al., 2017). Specifically, for each fiber f in a subject-specific cluster c, a Dice overlap score with the corresponding atlas cluster's TAP ($TAP_{atlas}(c)$) was computed, and the mean Dice score across all fibers was used to measure the TAPC of c, as:

$$TAPC(c) = \frac{\sum_{f=1}^{NF(c)} Dice(TAP(f), TAP_{atlas}(c))}{NF(c)} \quad (3)$$

where NF is the total number of fibers in the subject-specific cluster c. Equation 3 is the mean of the Dice overlap scores across all fibers within a subject-specific cluster, where a high value suggests a high anatomical coherence of the cluster.

3. Experiments and results

3.1. Coarse-to-fine scale whole brain white matter parcellations

We first performed experiments on the two HCP datasets (HCP-atlas and HCP-test) to investigate whole brain white matter parcellation at different scales. Specifically, we generated multiple fiber clustering atlases at different scales (k = 200 to 4000) using the HCP-atlas subjects (Section 2.2). Given the atlas at a certain scale, each subject from the two datasets was clustered accordingly to obtain subject-specific fiber clusters for a whole brain white matter parcellation (Section 2.4.1). The previously introduced quantitative measurements were then computed to evaluate the white matter parcellation generalization (WMPG), the inter-subject parcellation variability (ISPV) and the tract anatomical profile coherence (TAPC) (Section 2.5) for each scale atlas. We note that the two HCP datasets were analyzed separately for a goal of evaluations on the population used for the atlas generation and a separated testing population.

Figure 3a shows the parcellation generalization results, where the bar charts give the mean percentages of the successfully detected clusters across all subjects in each HCP dataset. While there were slight decreases in the fine scale parcellations (e.g. $K > 2000$), very high percentage values were obtained in both datasets across the multiple atlases, indicating that almost all clusters (over 98.7% across the multiple parcellation scales) could be successfully detected.

Figure 3b gives the results of the inter-subject variability evaluation. For each cluster, the CV of the number of fibers was computed across all subjects in each dataset. Then, the mean of the CV values across all clusters was reported for each parcellation scale, as shown by the bar charts in Figure 3b. A low CV value indicates a low variability hence a high consistency. The mean CV values increased from coarse to fine scale parcellations, while the changes

tended to be less obvious at finer scales (e.g. $K \geq 2000$) compared to the coarse scale parcellations (e.g. $K \geq 800$). Overall, across the multiple atlases under study, the mean CV values were lower than 0.64, with an averaged mean CV value of 0.53 in the two datasets.

Figure 3c displays the tract anatomical profile coherence results. For each subject-specific cluster per dataset, a Dice score was computed by comparing each fiber in this cluster to the corresponding atlas cluster in terms of the tract anatomical profile (Section 2.5.3). The averaged Dice score across all subjects in each dataset was computed for each individual cluster. Then, the mean of the averaged Dice across all clusters was reported as shown by the bar charts in Figure 3c. A high Dice score represents a high coherence between the subject cluster and the corresponding atlas cluster. The mean averaged Dice score increased dramatically before $k = 800$, followed by slight changes until $k = 2000$, and then tended to be stable after $k = 2000$. In general, a high Dice overlap score of around 0.8 was obtained across the multiple atlases under study.

Based on the above experiments, we chose $K = 800$ for a coarse-scale parcellation atlas and $K = 2000$ for a fine-scale parcellation atlas. These two atlases were used to evaluate subject-specific whole brain white matter parcellation in the multiple testing datasets (i.e. dHCP, ABIDE-II, CNP, PPMI and BTP), as described in the next section.

3.2. Whole brain white matter parcellations of the testing subjects

Here we describe experimental results from applications of the two selected fiber clustering atlases ($k = 800$ and 2000) to the testing subjects across different ages, genders and disease conditions (see Section 2.1.1 for demographics) for subject-specific whole brain white matter parcellations. Tables 4, 5 and 6 give the white matter parcellation generalization (WMPG), the inter-subject parcellation variability (ISPV) and the tract anatomical profile coherence (TAPC) evaluation results. For each population per parcellation scale, the WMPG, ISPV and TAPC values in the tables were calculated in the same way as in the above section, showing the mean percentages of the successfully detected clusters, the mean of the CV of number of fibers across all clusters, and the mean of the averaged Dice overlap scores across all clusters, respectively. For comparison, the corresponding values computed from the two HCP datasets were listed in the first two rows in each table. We note that the TAPC evaluation (Table 6) was not performed on the dHCP and BTP datasets due to the unavailability of Freesurfer segmentations in these two datasets.

Across the multiple testing datasets, high parcellation generalization results were obtained in the ABIDE-II, CNP and PPMI datasets (over 94% for the coarse scale and over 87% for the fine scale), shown in Table 4. For dHCP and BTP, although the subjects in these two datasets had largely different neuroanatomy to the atlas population, due to neurodevelopment and the presence of brain tumors, over 90% of the clusters were successfully detected for a coarse scale parcellation and over 76% were detected for a fine scale parcellation.

For the inter-subject variability results shown in Table 5, low CV values of the number of fibers (thus high inter-subject consistency) were obtained for the two adult testing datasets (i.e. CNP and PPMI). For the neonates and the children (i.e. dHCP and ABIDE-II), higher CV values were obtained compared to the adult subjects, suggesting higher inter-subject

variabilities. These were potentially because of the rapid brain development during the perinatal period and childhood. In addition, higher inter-subject variabilities could also be observed in the brain tumor patients (BTP), due to the effects of the patient-specific tumors.

Table 6 shows the tract anatomical profile coherence results. For the four testing datasets with available Freesurfer segmentations, similar averaged tract profile Dice overlap scores (around 0.75) were obtained. These values were similar to the ones from the two HCP datasets, suggesting that the obtained subject-specific clusters were highly coherent in terms of passing though common Freesurfer regions. For the dHCP and BTP datasets, their profile coherence measurements were not able to be computed due to the unavailability of Freesurfer segmentation.

Regarding the differences between the two parcellation scales, we could in general find that the coarse scale parcellation ($K = 800$) tended to have better parcellation generalization and inter-subject variability performances but slightly lower tract profile coherence results.

3.3. Anatomically curated white matter atlas for anatomical fiber tract identification

In this section, we show the results from applying the anatomically curated white matter atlas ($K = 800$) (Section 2.3) for anatomical tract identification, in the following two experiments.

3.3.1. Population-based anatomical tract visualization—We first performed an experiment to show a tract visualization from a population perspective for each dataset under study. The goal was to test if the proposed atlas could in general be applied for successful identification of common white matter structures, while allowing to capture the anatomical variabilities, across the different cohorts. To do this, given an anatomical tract annotated in the atlas, we combined the corresponding subject-specific tracts of all subjects in each dataset. Fibers from each combined tract were randomly downsampled for visualizations.

Figure 4 gives the population-based tract visualizations of several selected example tracts for each dataset. We first showed the tract visualizations of the two HCP cohorts that had matched ages and genders, scanned with the same diffusion imaging acquisitions. Visual comparisons showed highly similar population-based tracts between the two cohorts. Then, we gave the tract visualizations for the dHCP, the ABIDE-II, the CNP and the PPMI datasets that were composed of subjects from 1 day to 82 years old across multiple disease conditions as well as healthy controls. While each tract could be successfully identified to represent a common white matter structure, we could also observe anatomical variabilities across the different cohorts. For example, the AF tract of the neonate subjects (i.e. dHCP) had fewer fibers in the anterior section when compared to the adult subjects. Last, we also gave the population-tract visualizations of the BTP dataset. In general, we identified population-based tracts that were visually comparable to the other datasets. However, while subject-specific tumors were located in different regions, observable deformations due to brain tumor mass effect could be seen in certain regions. For example, half of 26 brain tumor patients under study had tumors and/or edema in the left hemisphere touching and affecting the left CST. Therefore, in Figure 4 (the CST tract in the last row), we could see observable deformations of this tract in the BTP dataset.

To assess the anatomical validity of the fiber tracts annotated in the atlas, we visualized the brain regions through which the fiber tracts pass. This was conducted by computing a voxel-based tract heatmap based on the 100 HCP-atlas subjects, where the value of each voxel in the heatmap represented the number of subjects that had fibers passing through the voxel. Figure 5a shows the tract heatmaps from three example tracts, overlaid on the population mean T1 image from all HCP-100 subjects (Section 2.2). Three example tracts including AF, CST and CC2 are displayed. We also provide the tract visualization for one individual HCP-atlas subject, with the tracts overlaid on the subject's T1 image, as shown in Figure 5b. In general, our identified tracts corresponded well to the known anatomy of the white matter pathways. The AF tract included the C-shaped fibers connecting the temporal, parietal, and frontal lobes (Catani and Mesulam, 2008). The CST passed through the midbrain, the posterior limb of the internal capsule, and then connected to primary motor, primary somatosensory, and dorsal premotor cortices, plus the supplementary motor area (Seo and Jang, 2013). The CC2 tract passed through the genu of the corpus callosum and connected to the bilateral frontal lobes (Makris et al., 1999).

3.3.2. Subject-specific tract identification—Next, we show tract identification results from individual subjects using the proposed anatomically curated white matter atlas. (See the supplementary material for the visualization of the tracts obtained using two additional tractography methods for these individual subjects.) For comparison, we performed a WMQL-based tract identification, which relied on a Freesurfer brain segmentation (as described in Section 2.3.1). Quantitative and visual comparisons were conducted, as follows.

For a quantitative comparison, we computed the white matter parcellation generalization (WMPG), the inter-subject parcellation variability (ISPV) and the tract anatomical profile coherence (TAPC) given the tracts identified in the two methods, as shown in Table 7. We first demonstrated the comparisons on the 45 deep white tracts (DT-45 tracts as listed in Table 7) which had available WMQL definitions (Section 2.3.1). For the parcellation generalization result, both methods showed good tract identification result by detecting over 99% of the tracts in all subjects in the HCP-atlas, the HCP-test, the dHCP, the ABIDE-II, the CNP and the PPMI datasets. In the dHCP and the BTP datasets, the WMQL method could not work because of the unavailability of Freesurfer segmentations. However, our proposed method detected 99.56% of tracts in the dHCP dataset and over 95% in the BTP dataset. For inter-subject variability, our method obtained a lower mean CV of number of fibers compared to WMQL, suggesting a higher inter-subject consistency obtained using the proposed method. For tract profile coherence, while our method did not rely on any Freesurfer information of the testing subjects, we still obtained similar (relatively lower) averaged tract profile Dice scores to the WMQL method.

In addition to the above 45 tracts, in Table 7 we also listed the parcellation generalization, the inter-subject variability and the tract profile coherence results from the tracts that were identified using our method but not defined in WMQL. These included the 13 deep white matter tracts (DT-13 tracts as listed in Table 7) including the cerebellar tracts and the corona radiata (excluding the CST) tracts, and the 198 superficial fiber tracts (ST-198 tracts as listed in Table 7). In general, the performance on the 13 deep white matter structures (DT-13) was

similar to the above 45 deep white matter tracts (DT-45), and the performance on the superficial tracts was high, but slightly lower than the deep white matter tracts.

For visual comparison, we showed several example tracts from individuals for each dataset, as displayed in Figure 6. We selected multiple example individuals from the datasets under study, with the purpose of including subjects across different the age ranges, the genders and the disease conditions. For our method, we also provided visualizations of two example tracts that were not defined in WMQL. In general, the two methods obtained comparable visualization of the identified tracts. However, specific differences could be observed. For example, our method was able to exclude some apparent outlier fibers (e.g. in SLF II and CC4).

4. Discussion

In this paper, we proposed an anatomically curated fiber clustering white matter atlas to enable whole brain white matter parcellation and anatomical tract identification consistently across multiple populations. We first showed that the data-driven fiber clustering method allowed for consistent whole brain white matter parcellation across subjects at coarse to fine scales from $K = 200$ to 4000 (Figure 3). We selected two reasonable fiber clustering atlases for coarse scale ($K = 800$) and fine scale ($K=2000$) whole brain white matter parcellations. We chose the coarse scale parcellation ($K = 800$) to create the anatomically curated white matter atlas for tract identification. The uncurated data-driven parcellation ($K = 2000$) is made available for applications that can benefit from a finer scale parcellation. We proposed a novel fiber cluster anatomical annotation method that leveraged population-based brain anatomical information and expert neuroanatomical assessment. Given the chosen whole brain parcellation scale into 800 fiber clusters, most clusters were annotated (82.5 % of all clusters), including both known white matter anatomy tracts (63.75% of all clusters) and potential false positive tracts (18.75% of all clusters). A relatively large number (256) of white matter structures were annotated in the proposed atlas, including fiber tracts from the entire brain. Most previous neuroscientific investigations have been limited to a small set of major fiber pathways (Mori et al., 2009; Varentsova et al., 2014; Pecheva et al., 2017), lacking a comprehensive coverage of the entire brain (including cerebellum, brainstem and superficial tracts).

The selection of the two fiber clustering atlases corresponded well to findings in previous works. Optimal white matter subdivision depends on the desired application (such as visualization, which can benefit from fewer clusters, or quantitative measurement, which can benefit from finer subdivisions thus more clusters). In one of our previous fiber-clustering-based studies, we empirically determined a value ($K = 800$) that could separate white matter structures considered to be anatomically different for an anatomical tract visualization task (O'Donnell et al., 2017). In another study, we also applied this value to perform between-population statistical analysis (Zhang et al., 2018b). On the other hand, our other research work suggested that parcellation of the whole brain white matter into a large number of fiber clusters (K from 2000 to 2800) tended to increase the performance in a machine-learning-based classification task (Zhang et al., 2018a), and could be beneficial in modeling whole brain structural connectivity (Zhang et al., 2017a).

We demonstrated successful applications of the anatomically curated white matter atlas for subject-specific anatomical tract identification. Over 99% anatomical tracts annotated in the atlas could be successfully identified in all testing datasets (Table 7). In the BTP dataset consisting of 26 brain tumor patients, there were 15 patients having at least one missing tract, resulting in a small percent of missing tracts (2.9%) from a total of 1924 (26×(58+16)) tracts. For example, one patient had a tumor and edema across the left temporal, insular, parietal and occipital lobes, where the tractography method tracked few fibers. Therefore, tracts such as striato-occipital (SO), thalamo-occipital (TO) and superficial tracts between the occipital and temporal lobes (Sup-OT) were not detected in this patient.

While enabling consistent white matter tract parcellation across the multiple testing datasets, the proposed atlas also allowed for capturing population-specific brain anatomical characteristics related to neurodevelopment. For example, in our population-based tract visualization results (Figure 4), the identified arcuate fasciculus (AF) tracts in the neonate subjects had fewer fibers in the anterior segment when compared to the adult subjects, which corresponds to the anatomical knowledge that neonates have incomplete development of the AF tract (Tak et al., 2016). In a second example of population-specific characteristics related to neurodevelopment, we found higher inter-subject parcellation variabilities on the dHCP (neonates) and ABIDE-II (children) datasets compared to the CNP and PPMI datasets (adults) (Tables 5 and 7). This could be explained by the fact that compared to adults whose brains are relatively mature, the brain develops rapidly during the perinatal period and childhood, leading to a larger inter-subject brain anatomical variability.

We showed the proposed white matter atlas's high performance to parcellate white matter tracts across populations despite the heterogeneity of the diffusion MRI data. Our testing data was independently acquired using different scanning protocols (such as b-values, spatial resolution and number of gradient directions) and processed in different manners. These factors could affect the tractography results and thus influence the parcellation generalizations between different datasets. However, despite any potential effects from the heterogeneity of the diffusion MRI data, we showed excellent parcellation generalization performance across the multiple testing datasets, with over 95.7% of the 800 fiber clusters (Table 4), and nearly 100% of the annotated anatomical fiber tracts (Table 7), successfully identified across all 584 testing subjects. There were still some remaining differences across populations that may relate to the dataset heterogeneity. For example, in our quantitative comparison results in terms of parcellating the whole brain white matter into fiber clusters (Table 4), we could see that relatively lower generalization performances were obtained on the multiple testing datasets compared to the two HCP datasets. Another example potentially related to data heterogeneity was that, from the subject-specific tract visualization results (Figure 6), we could observe that the CNP subjects had very few fibers in the yellow and orange clusters of the corticospinal tract. This could indicate that tracking through crossing fiber regions was more challenging using diffusion MRI data from the CNP dataset.

Comparisons to a WMQL-based tract identification method showed several benefits of the proposed method, as follows. First, our method used only tractography data for subject-specific tract identification, without relying on the success of cortical or subcortical segmentations. Therefore, our method could be in general applied to individuals with large

brain anatomical variations. For example, we showed successful tract identification in neonate subjects whose brain anatomy is well-known to be different from that of adult subjects (Shi et al., 2011; Makropoulos et al., 2017a), and in brain tumor patients who had distorted white matter structures due to the mass effect of the brain tumor (O'Donnell et al., 2017). We note that a Freesurfer segmentation could not in general be conducted in these cohorts, and thus a WMQL-based tract identification failed. Second, a lower inter-subject variability in terms of the number of fibers in the tracts was obtained in our method compared to WMQL (Table 7). The WMQL method depended on how the fibers intersected with the segmented Freesurfer regions, and thus was sensitive to whether the fibers' endpoints touched target segmented regions (mostly gray matter regions). However, the proposed method was based on a fiber clustering pipeline that used the full length of the fiber trajectory. This could enable a more robust tract identification by incorporating fibers whose endpoints did not quite reach gray matter regions, e.g. near the cortex where a low diffusion anisotropy was present. Third, our proposed method could better reject apparent outlier fibers compared to the WMQL (e.g. the CC4 tract in Figure 6). This was due to the inclusion of an outlier removal process when performing the fiber clustering (Section 2.4.1). The groupwise fiber trajectory-based computation could naturally enable the rejection of the fibers that were improbable (trajectory-dissimilar) in the cluster.

The proposed atlas-based white matter parcellation method aimed to address the known issue of false positive tracts. In this study, we applied a multi-fiber tractography method to increase the sensitivity in tracking crossing fibers (Baumgartner et al., 2012; Chen et al., 2015, 2016; Liao et al., 2017). The high sensitivity has been suggested to be important to reduce false negatives, but at the expense of increased false positives (Maier-Hein et al., 2016; Thomas et al., 2014). Therefore, the applied highly sensitive UKF fiber tracking method may introduce more false positive or anatomically incorrect errors compared to a standard single-fiber diffusion tensor fiber tracking method. In our method, we included two solutions to remove any possible false positive fibers. First, as discussed above, we included an outlier removal process to reject improbable fibers within a cluster. While this process could ameliorate the false positive fibers to a certain extent, it could not remove tractography errors that were present in all subjects while being inconsistent with expected anatomy. For instance, we found fiber clusters connecting the cortex and cerebellum in the same hemisphere in the atlas fiber clustering results. To handle such tractography errors, during the expert judgment, we annotated in the atlas potential false positive clusters such as the intra-hemispheric cerebellum tracts and partially traced corpus callosum tracts. This can enable the exclusion of such clusters in downstream processing and visualization.

Potential future directions and limitations of the current work are as follows. First, because fiber clusters were formed based on fiber geometric properties only, fibers at boundary regions between different anatomical white matter structures could be grouped into one cluster. In our proposed atlas, we assigned such a cluster to an anatomical tract that the cluster's fibers primarily belonged to. This could result in a tract containing several inter-tract fibers. For example, the CST is considered to include the ascending fibers that pass through the middle third of the cerebral peduncle (Haines, 2004), but our atlas tended to be over-inclusive by including descending fibers that pass through the region posterior to the middle third of cerebral peduncle. It is well known issue in tractography that it cannot

distinguish such directional fibers (Maier-Hein et al., 2017). As a result, our fiber clustering method grouped them together because their fiber geometric trajectories were very similar. A possible solution is to include additional brain anatomy information (e.g. the Freesurfer segmentation) when forming the fiber clusters, as applied in many fiber clustering works (Xia et al., 2005; Li et al., 2010; Tunç et al., 2013; Wang et al., 2013; Ros et al., 2013; Siless et al., 2018). However, this would largely complicate the application to individuals where such additional information was not available, e.g. neonates and brain tumor patients. Second, the aim of this study was to demonstrate the applications of the proposed atlas for whole brain white matter parcellation and anatomical tract identification. While we focused on demonstrating successful applications across the different cohorts, we did not perform any statistical analyses for within- or between-cohort studies. The proposed method, in conjunction with approaches to harmonize diffusion MRI measurements across scanners (Mirzaalian et al., 2016; Zhang et al., 2016), can enable such studies to compare white matter tracts across the lifespan. Third, for the atlas generation, we applied the UKF tractography method that has shown advantages (e.g. tracking through crossing fiber regions and edema) in our multiple studies (Baumgartner et al., 2012; Chen et al., 2015, 2016; Liao et al., 2017). However, in recent years, many new tractography methods (such as global (Christiaens et al., 2015) and multi-tissue (Jeurissen et al., 2014) fiber tracking methods) have been proposed, which potentially could be used to generate improved atlases. In an initial experiment, we have shown successful applications of the atlas to tractography data computed using different fiber tracking methods, including diffusion tensor tractography and constrained spherical deconvolution tractography (see the supplementary material). Although these tractography data vary quite significantly given different fiber tracking models and different parameters such as fiber angle and step size, as well as the output number of fibers, we showed that our overall pipeline including the data-driven fiber clustering and the anatomically curated atlas in general allowed for identification of anatomical tracts that were visually plausible. An interesting future work could include comparing the differences of white matter structures identified from different tractography methods. Fourth, to demonstrate the anatomical validity of the proposed atlas, we showed that our identified tracts corresponded well to the known anatomy of the white matter pathways in the brain in several example well-established deep brain white matter tracts (Figure 5). As for the superficial fiber tracts, which include fibers near the cortex (Oishi et al., 2008; Guevara et al., 2017), we showed good performance in detecting them consistently across multiple populations (Table 7). Over 93% of the superficial fiber clusters were identified in all subjects across all datasets, and over 98% in many datasets, suggesting that it is feasible to identify and study a large number of superficial connections. The superficial white matter structures in the brain are not as well studied as the deep brain white matter structures due to their small size, high structural complexity, and high inter-subject variability (Oishi et al., 2008; Guevara et al., 2017). A future study could provide a more comprehensive anatomical validation about the annotated superficial tracts in the atlas. Fifth, future white matter atlas creation work could leverage approaches for reducing image distortion in the brainstem in HCP data (Irfanoglu et al., 2015; Tang et al., 2018). Finally, in the current atlas, we have provided rough categories for the superficial fibers (according to the different brain lobes the fibers connect) and the cerebellar fibers (e.g. the cortico-ponto-cerebellar tract and the intracerebellar tract). In addition, 17.5% of the clusters have not been

categorized. Investigation into sub-categories of these structures, to provide additional detail to the annotations in the atlas, would be an interesting future work.

5. Conclusion

In this paper, we have presented an anatomically curated fiber clustering white matter atlas to enable white matter tract parcellation. Experimental results show successful application of the proposed atlas for consistent whole brain white matter parcellation and anatomical tract identification of subjects across the full lifespan and across multiple MRI acquisition protocols.

Supplementary Material

Refer to Web version on PubMed Central for supplementary material.

Acknowledgements

We would like to thank Drs. Alexandra Golby, Walid I. Essayed, and Prashin Unadkat for their great help on this project. We gratefully acknowledge funding provided by the following National Institutes of Health (NIH) grants: P41 EB015902, P41 EB015898, R01 MH074794, R01 MH097979, U01 CA199459, and R03 NS088301.

Appendix A.: Data preprocessing and UKF tractography

For the two HCP datasets, we used the already processed diffusion MRI data (following the processing pipeline in (Glasser et al., 2013)). We extracted the b = 3000 shell of 90 gradient directions and all b = 0 scans for each subject, as applied in our previous studies (O'Donnell et al., 2017; Zhang et al., 2017b,a). Angular resolution is better and more accurate at high b-values such as 3000 (Descoteaux et al., 2007; Ning et al., 2015), and this single shell was chosen for reasonable computation time and memory use when performing tractography. The Freesurfer segmentation results were directly used.

For the dHCP datasets, we used the already processed diffusion MRI data (following the processing pipeline in (Makropoulos et al., 2017b)). Unlike the adult HCP dataset (where only high b = 3000 shell was used), we kept all the gradient directions based on our visual inspection that a high b shell tended to be very noisy in the dHCP dataset. Due to difficulties in the translation of conventional adult methods for image processing to neonatal cohorts, the Freesurfer brain segmentation could not be computed for the dHCP dataset (Makropoulos et al., 2017b).

For the ABIDE-II, the CNP and the PPMI datasets, we pre-processed the provided raw imaging data using the following steps. DWIConvert[7] was first applied to convert the original data format (DICOM or NIFTI) to NRRD. Eddy current-induced distortion correction and motion correction were conducted using the Functional Magnetic Resonance Imaging of the Brain (FMRIB) Software Library tool (Jenkinson et al., 2012). To further correct for distortions caused by magnetic field inhomogeneity (which leads to intensity loss and voxel shifts), an EPI distortion correction was performed with reference to the T2-

[7] https://github.com/BRAINSia/BRAINSTools

weighted image using the Advanced Normalization Tools (ANTS) (Avants et al., 2009). Because T2-weighted images were not available in all of these datasets (no T2 images were provided in the ABIDE-II and the CNP datasets, and in the PPMI dataset not all subjects had T2 images), we generated a synthetic T2-weighted image from a T1-weighted image for each subject (T1 images were available for in all datasets) using the T1 to T2 conversion toolbox[8]. For each subject, a nonlinear registration (registration was restricted to the phase encoding direction) was computed from the b0 image to the synthetic T2-weighted image to make an EPI corrective warp. Then, the warp was applied to each diffusion image. A semi-automated quality control (using in-house developed Matlab scripts) was conducted on all diffusion images. Individuals that had diffusion images with any apparent signal drops were excluded from the analyses. For the remaining subjects, all gradient directions were retained for analysis. We also performed a Freesurfer segmentation for each subject in these three datasets. Each individual's Freesurfer segmentation was transformed from T1 space into diffusion corrected (b0) space via nonlinear registration using ANTS.

For the BTP dataset, we followed processing steps tuned specifically for brain tumor patient data, as reported in (O'Donnell et al., 2017). Diffusion images were corrected for motion and eddy current distortions using DTIPrep (Oguz et al., 2014). Images from all gradient directions were retained based on visual inspection of several patient datasets with an in-house tool indicating no gradients should be removed. Thus, all 30 gradient directions were retained for analysis. Our attempts using the FreeSurfer software on the patient data failed to output a final brain segmentation on most subjects due to the influence of the tumors. Therefore, we did not include any Freesurfer results for the BTP dataset.

After obtaining the pre-processed DWI data, we applied the same UKF parameters for all subjects under study, as follows. Tractography was seeded in all voxels within the brain mask where fractional anisotropy (FA) was greater than 0.1. Tracking stopped where the FA value fell below 0.08 or the normalized mean signal (the sum of the normalized signal across all gradient directions) fell below 0.06. The normalized average signal measure was employed to robustly distinguish between white/gray matter and cerebrospinal fluid (CSF) regions. These seeding and stopping thresholds were set slightly below the default values to enable higher sensitivity for fiber tracking, in particular for the subjects (such as neonates, children and brain tumor patients) that might have low white matter anisotropy. Fibers that were longer than 40 mm were retained to avoid any bias towards implausible short fibers (Guevara et al., 2012; Jin et al., 2014; Lefranc et al., 2016).

Appendix B.: Fiber clustering atlas generation

Here, we provide a brief introduction of the pipeline for the fiber clustering atlas generation. The pipeline begins with computing an unbiased groupwise whole brain tractography registration to simultaneously align all subjects' tractography into a common space (i.e. atlas space) (O'Donnell et al., 2012). The method performs an entropy-based registration in a multiscale manner based on the pairwise fiber trajectory distances (the popular mean closest point distance is used (Moberts et al., 2005; O'Donnell and Westin, 2007)) across all

[8] https://github.com/pnlbwh/T1toT2conversion

subjects. The registration method has been applied in multiple studies that have shown the success of the method in enabling consistent white matter parcellation across subjects (O'Donnell et al., 2017; Zhang et al., 2017a,b, 2018a,b; Gong et al., 2018; Sydnor et al., 2018; Wu et al., 2018). Next, spectral embedding is used to compute a high-dimensional fiber clustering atlas (O'Donnell and Westin, 2007) to divide the whole brain tractography into K clusters (K is a user-given parameter to define parcellation scale), as follows. The spectral embedding creates a space that robustly represents each fiber according to its affinity to all other fibers across subjects. The fiber affinity is computed by converting pairwise fiber geometric distances (same as used in the tractography registration) using a Gaussian-like kernel with sigma of 60 mm, representing fiber similarity according the white matter anatomy. Nystrom sampling (Fowlkes et al., 2004) is used to reduce the computations considering the large number of fiber pairs across subjects. Bilateral clustering, simultaneously segmenting fibers in both hemispheres to improve parcellation robustness (O'Donnell and Westin, 2007), is applied to obtain the K fiber clusters.

Appendix C.: Tract anatomical profile (TAP) and TAP coherence (TAPC)

The tract anatomical profile (TAP) of an atlas cluster ($TAP_{atlas}(c)$) was defined as the set of brain regions most highly intersected by the cluster (the set of brain regions through which the cluster passed consistently) across the 100 HCP-atlas subjects, as illustrated in Figure Appendix C.1(a). To describe the possibility of a segmented region r belonging to the tract profile of an atlas cluster c, we computed a population-based percentage of r given c, i.e. $P(r/c)$, as follows. First, we identified the fibers that passed through the region r in the cluster c in each HCP-atlas subject. Then, we calculated the percentage of these identified fibers over the total number of fibers in c across the 100 subjects, yielding $P(r/c)$.

A percentage threshold Th was then used to determine if r belonged to the TAP of c, i.e. $P(r/c) \geq Th$. The goal of the threshold is to identify a TAP that represents the population characteristics of the cluster. A too-high Th value would include too few regions into the TAP, while a too-low Th value would be overinclusive. To investigate the effect of Th, we applied the tract anatomical profile coherence (TAPC) measurement (defined in Section 2.5.3) given the TAPs obtained under different Th values (30% to 80%). The TAPC measurement evaluated if the fibers within a cluster commonly passed through the same brain regions (according to the TAP of the cluster). It was measured by computing the Dice overlap score (see Section 2.5.3 for details) between the brain regions though which each fiber passed and those in the cluster's TAP, where a high value indicated fibers within the cluster were highly coherent. Here, given a cluster c, we calculated a Dice score for each HCP-atlas subject and computed an average Dice score across the 100 subjects. Then, the mean of the averaged Dice scores was reported across all clusters.

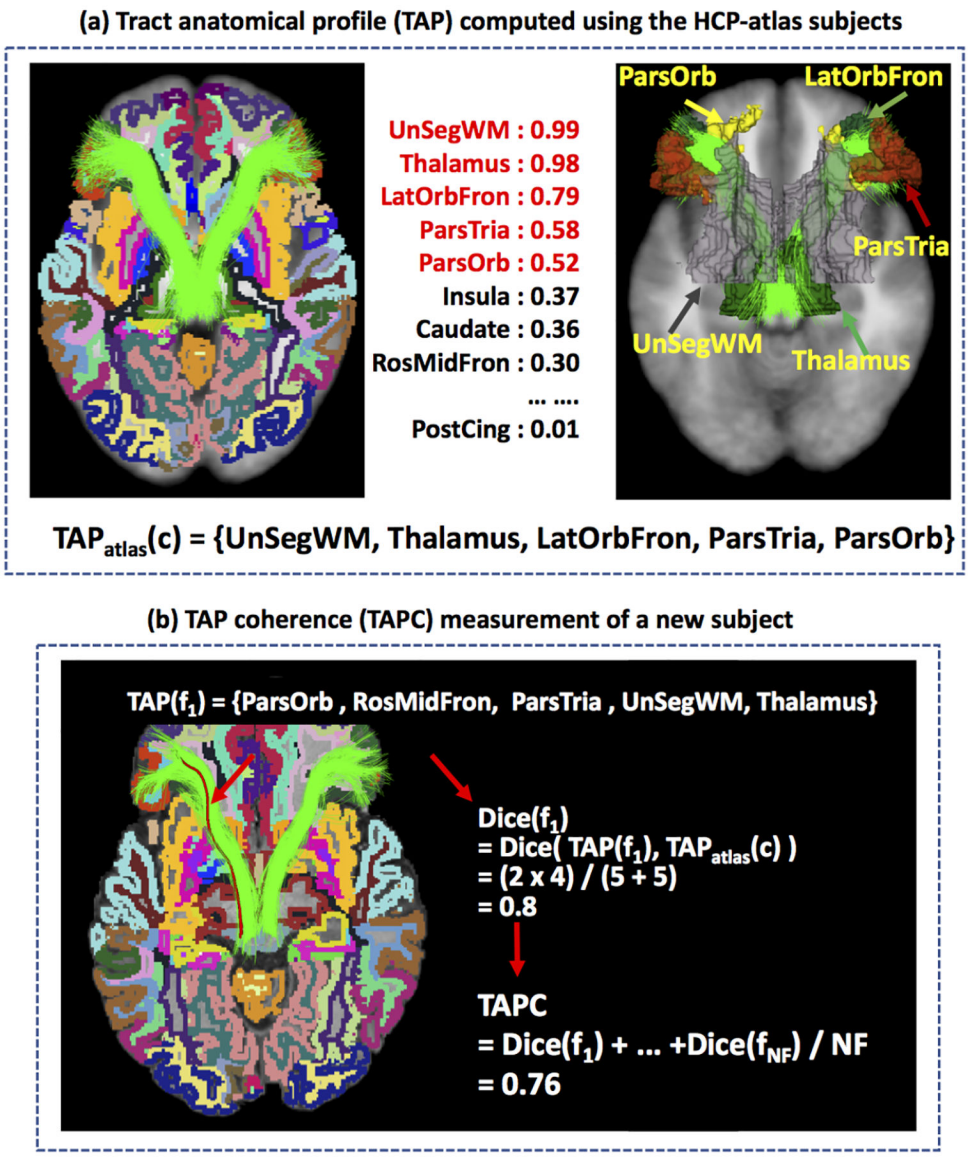

Figure Appendix C.1:

(a) Overview of the computation of the TAP$_{atlas}$ of one atlas cluster *c*. This process used the full clustered tractography data (approximately 1 million fibers per subject) from the 100 HCP-atlas subjects (Section 2.1.1). For each Freesurfer segmented region, the percentage of fibers in *c* that intersect this region (across the 100 subjects) is computed. A high percentage value indicates that a Freesurfer segmented region is highly intersected by the cluster across all subjects. Then, a threshold (see Figure Appendix C.2) is applied to this percentage to determine the set of most highly intersected regions, i.e. the TAP of the atlas cluster (TAP$_{atlas}$(*c*)). As an example, the sample atlas cluster has a TAP containing five Freesurfer regions (as listed in the figure). (b) Illustration of the computation of TAPC (TAP coherence) for a subject-specific cluster. For each fiber f within the cluster, the set of Freesurfer regions through which the fiber passes is measured. This gives the TAP of the fiber (TAP(*f*)). Then, a Dice score between the fiber's TAP (TAP(*f*)) and the atlas cluster's TAP (TAP*atlas*) is

computed. For example, the sample fiber (red) has a Dice score of 0.73. Then, the TAPC is calculated as the mean Dice score across all fibers in the subject-specific cluster.

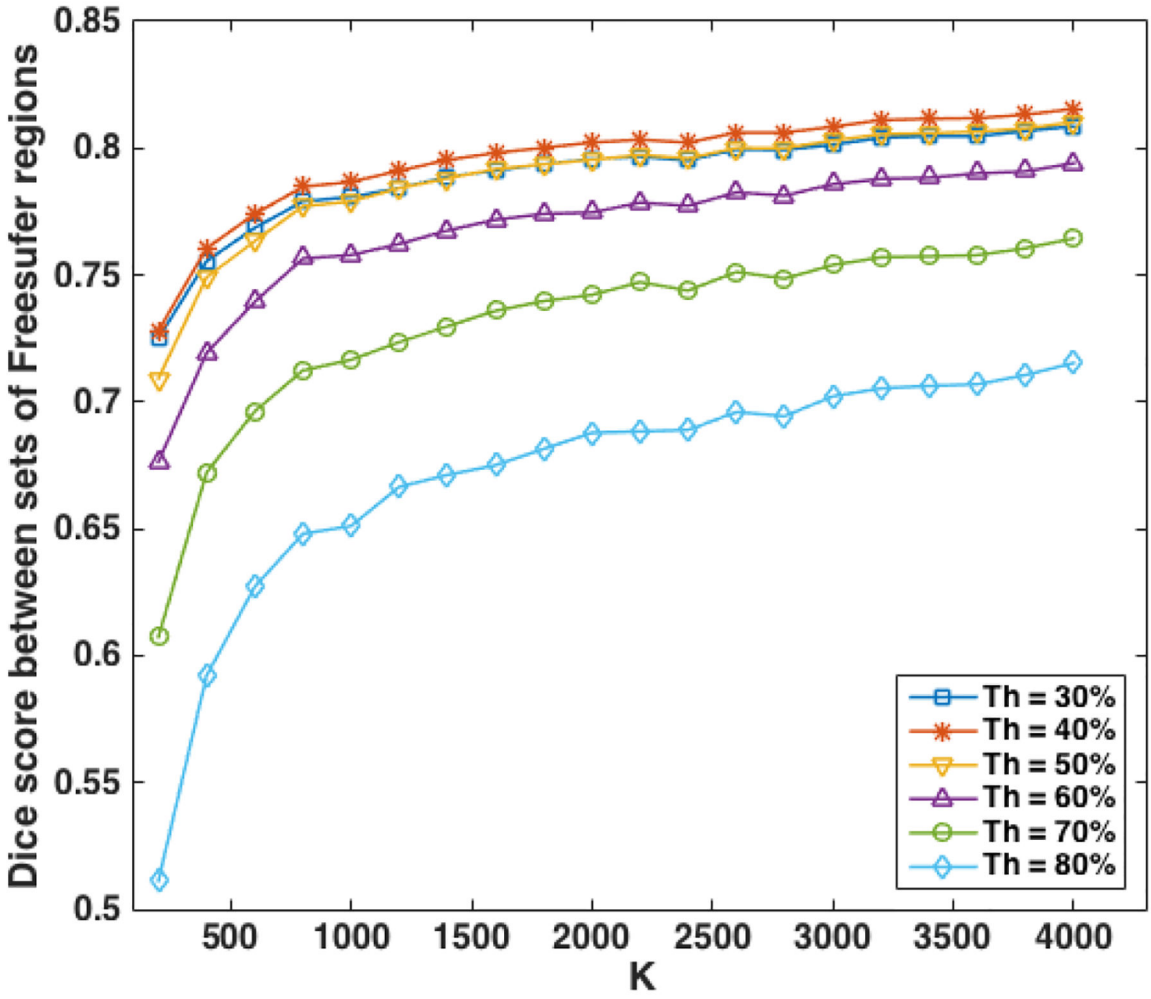

Figure Appendix C.2:
Threshold determination for defining tract anatomical profile. *Th* = 40% generated the highest Dice scores across the different settings under different parcellation scales.

Figure Appendix C.2 shows the mean averaged Dice scores under different *Th* values given multiple parcellation scales. The value *Th* = 40% generated the highest Dice scores across the different settings. Therefore, in our study, we chose the threshold of 40% when determining the TAP of the clusters in the atlas.

The TAP coherence was measured for a subject-specific cluster by computing the mean of the Dice overlap score between each subject-specific fiber's TAP (TAP(*f*)) and the atlas cluster's TAP ($TAP_{atlas}(c)$), as illustrated in Figure Appendix C.1 (b).

References

Akazawa K , Chang L , Yamakawa R , Hayama S , Buchthal S , Alicata D , Andres T , Castillo D , Oishi K , Skranes J , Ernst T , Oishi K , 2016 Probabilistic maps of the white matter tracts with known associated functions on the neonatal brain atlas: application to evaluate longitudinal developmental trajectories in term-born and preterm-born infants. NeuroImage 128, 167–179.26712341

Alexander AL , Lee JE , Lazar M , Boudos R , DuBray MB , Oakes TR , Miller JN , Lu J , Jeong E-K , McMahon WM , Bigler ED , Lainhart JE , 2007 Diffusion tensor imaging of the corpus callosum in Autism. NeuroImage 34 (1), 61–73.17023185

Amunts K , Schleicher A , Bürgel U , Mohlberg H , Uylings H , Zilles K , 1999 Broca's region revisited: cytoarchitecture and intersubject variability. Journal of Comparative Neurology 412 (2), 319–341.10441759

Avants BB , Tustison N , Song G , 2009 Advanced normalization tools (ANTS). Insight j 2, 1–35.

Basser PJ , Mattiello J , LeBihan D , 1994 MR diffusion tensor spectroscopy and imaging. Biophysical Journal 66 (1), 259–267.8130344

Basser PJ , Pajevic S , Pierpaoli C , Duda J , Aldroubi A , 2000 In vivo fiber tractography using DT-MRI data. Magnetic Resonance in Medicine 44 (4), 625–632.11025519

Bassett DS , Bullmore ET , 2017 Small-world brain networks revisited. The Neuroscientist 23 (5), 499–516.

Bastiani M , Shah NJ , Goebel R , Roebroeck A , 2012 Human cortical connectome reconstruction from diffusion weighted MRI: the effect of tractography algorithm. NeuroImage 62 (3), 1732–1749.22699045

Baumgartner C , Michailovich O , Levitt J , Pasternak O , Bouix S , Westin C-F , Rathi Y , 2012 A unified tractography framework for comparing diffusion models on clinical scans. In: Computational Diffusion MRI Workshop of International Conference on Medical Image Computing and Computer Assisted Intervention pp. 27–32.

Bazin P-L , Ye C , Bogovic JA , Shiee N , Reich DS , Prince JL , Pham DL , 2011 Direct segmentation of the major white matter tracts in diffusion tensor images. NeuroImage 58 (2), 458–468.21718790

Brown JA , Terashima KH , Burggren AC , Ercoli LM , Miller KJ , Small GW , Bookheimer SY , 2011 Brain network local interconnectivity loss in aging APOE-4 allele carriers. Proceedings of the National Academy of Sciences 108 (51), 20760–20765.

Bullmore E , Sporns O , 2009 Complex brain networks: graph theoretical analysis of structural and functional systems. Nature Reviews Neuroscience 10 (3), 186–198.19190637

Calabrese E , Badea A , Coe CL , Lubach GR , Styner MA , Johnson GA , 2014 Investigating the tradeoffs between spatial resolution and diffusion sampling for brain mapping with diffusion tractography: time well spent? Human Brain Mapping 35 (11), 5667–5685.25044786

Catani M , De Schotten MT , 2008 A diffusion tensor imaging tractography atlas for virtual in vivo dissections. Cortex 44 (8), 1105–1132.18619589

Catani M , Mesulam M , 2008 The arcuate fasciculus and the disconnection theme in language and aphasia: history and current state. Cortex 44 (8), 953–961.18614162

Chen Z , Tie Y , et al., 2015 Reconstruction of the arcuate fasciculus for surgical planning in the setting of peritumoral edema using two-tensor unscented Kalman filter tractography. NeuroImage: Clinical 7, 815–822.26082890

Chen Z , Tie Y , Olubiyi O , Zhang F , Mehrtash A , Rigolo L , Kahali P , Norton I , Pasternak O , Rathi Y , Golby AJ , O'Donnell LJ , 2016 Corticospinal tract modeling for neurosurgical planning by tracking through regions of peritumoral edema and crossing fibers using two-tensor unscented Kalman filter tractography. International Journal of Computer Assisted Radiology and Surgery 11 (8), 1475–1486.26762104

Christiaens D , Reisert M , Dhollander T , Sunaert S , Suetens P , Maes F , 2015 Global tractography of multi-shell diffusion-weighted imaging data using a multi-tissue model. Neuroimage 123, 89–101.26272729

Ciccarelli O , Catani M , Johansen-Berg H , Clark C , Thompson A , 2008 Diffusion-based tractography in neurological disorders: concepts, applications, and future developments. The Lancet Neurology 7 (8), 715–727.18635020

Cousineau M , Jodoin P-M , Garyfallidis E , Côté M-A , Morency FC , Rozanski V , Grand'Maison M , Bedell BJ , Descoteaux M , 2017 A test-retest study on Parkinson's PPMI dataset yields statistically significant white matter fascicles. NeuroImage: Clinical 16, 222–233.

de Schotten MT , Bizzi A , Dell'Acqua F , Allin M , Walshe M , Murray R , Williams SC , Murphy DG , Catani M , 2011 Atlasing location, asymmetry and inter-subject variability of white matter tracts in the human brain with MR diffusion tractography. NeuroImage 54 (1), 49–59.20682348

Descoteaux M , Angelino E , et al., 2007 Regularized, fast, and robust analytical Q-ball imaging. Magnetic Resonance in Medicine 58 (3), 497–510.17763358

Di Martino A , O'Connor D , Chen B , Alaerts K , Anderson JS , Assaf M , Balsters JH , Baxter L , Beggiato A , Bernaerts S , Blanken LME , Bookheimer SY , Braden BB , Byrge L , Castellanos FX , Dapretto M , Delorme R , Fair DA , Fishman I , Fitzgerald J , Gallagher L , Keehn RJJ , Kennedy DP , Lainhart JE , Luna B , Mostofsky SH , Mller R-A , Nebel MB , Nigg JT , O'Hearn K , Solomon M , Toro R , Vaidya CJ , Wenderoth N , White T , Craddock RC , Lord C , Leventhal B , Milham MP , 2017 Enhancing studies of the connectome in autism using the autism brain imaging data exchange II. Scientific Data 4, 170010.28291247

Dice LR , 1945 Measures of the amount of ecologic association between species. Ecology 26 (3), 297–302.

Ding Z , Gore JC , Anderson AW , 2003 Classification and quantification of neuronal fiber pathways using diffusion tensor MRI. Magnetic Resonance in Medicine 49 (4), 716–721.12652543

Drakesmith M , Caeyenberghs K , Dutt A , Lewis G , David A , Jones DK , 2015 Overcoming the effects of false positives and threshold bias in graph theoretical analyses of neuroimaging data. NeuroImage 118, 313–333.25982515

Essayed WI , Zhang F , Unadkat P , Cosgrove GR , Golby AJ , O'Donnell LJ , 2017 White matter tractography for neurosurgical planning: A topography-based review of the current state of the art. NeuroImage: Clinical 15, 659–672.

Fischl B , 2012 FreeSurfer. NeuroImage 62 (2), 774–781.22248573

Fischl B , Sereno MI , Tootell RB , Dale AM , 1999 High-resolution intersubject averaging and a coordinate system for the cortical surface. Human Brain Mapping 8 (4), 272–284.10619420

Fowlkes C , Belongie S , Chung F , Malik J , 2004 Spectral grouping using the Nystrom method. IEEE Transactions on Pattern Analysis and Machine Intelligence 26 (2), 214–225.15376896

Garyfallidis E , Brett M , Correia MM , Williams GB , Nimmo-Smith I , 2012 Quickbundles, a method for tractography simplification. Frontiers in Neuroscience 6.

Garyfallidis E , Côté M-A , Rheault F , Sidhu J , Hau J , Petit L , Fortin D , Cunanne S , Descoteaux M , 2017 Recognition of white matter bundles using local and global streamline-based registration and clustering. NeuroImage, in press.

Glasser MF , Sotiropoulos SN , et al., 2013 The minimal preprocessing pipelines for the Human Connectome Project. NeuroImage 80, 105–124.23668970

Golby AJ , Kindlmann G , Norton I , Yarmarkovich A , Pieper S , Kikinis R , 2011 Interactive diffusion tensor tractography visualization for neurosurgical planning. Neurosurgery 68 (2), 496–505.21135713

Gong G , He Y , Concha L , Lebel C , Gross DW , Evans AC , Beaulieu C , 2009 Mapping anatomical connectivity patterns of human cerebral cortex using in vivo diffusion tensor imaging tractography. Cerebral Cortex 19 (3), 524–536.18567609

Gong S , Zhang F , Norton I , Essayed WI , Unadkat P , Rigolo L , Pasternak O , Rathi Y , Hou L , Golby AJ , O'Donnell LJ , 2018 Free water modeling of peritumoral edema using multi-fiber tractography: Application to tracking the arcuate fasciculus for neurosurgical planning. PloS one 13 (5), e0197056.29746544

Guevara M , Román C , Houenou J , Duclap D , Poupon C , Mangin JF , Guevara P , 2017 Reproducibility of superficial white matter tracts using diffusion-weighted imaging tractography. NeuroImage 147, 703–725.28034765

Guevara P , Duclap D , Poupon C , Marrakchi-Kacem L , Fillard P , Le Bihan D , Leboyer M , Houenou J , Mangin J-F , 2012 Automatic fiber bundle segmentation in massive tractography datasets using a multi-subject bundle atlas. NeuroImage 61 (4), 1083–1099.22414992

Hagler DJ , Ahmadi ME , Kuperman J , Holland D , McDonald CR , Halgren E , Dale AM , 2009 Automated white-matter tractography using a probabilistic diffusion tensor atlas: Application to temporal lobe epilepsy. Human Brain Mapping 30 (5), 1535–1547.18671230

Haines DE , 2004 Neuroanatomy: An atlas of structures, sections, and systems. Vol. 153 Lippincott Williams & Wilkins.

Hua K , Zhang J , Wakana S , Jiang H , Li X , Reich DS , Calabresi PA , Pekar JJ , van Zijl PC , Mori S , 2008 Tract probability maps in stereotaxic spaces: analyses of white matter anatomy and tract-specific quantification. NeuroImage 39 (1), 336–347.17931890

Ingalhalikar M , Smith A , Parker D , Satterthwaite TD , Elliott MA , Ruparel K , Hakonarson H , Gur RE , Gur RC , Verma R , 2014 Sex differences in the structural connectome of the human brain. Proceedings of the National Academy of Sciences 111 (2), 823–828.

Irfanoglu MO , Modi P , Nayak A , Hutchinson EB , Sarlls J , Pierpaoli C , 2015 DR-BUDDI (Diffeomorphic Registration for Blip-Up blip-Down Diffusion Imaging) method for correcting echo planar imaging distortions. NeuroImage 106, 284–299.25433212

Jenkinson M , Beckmann CF , Behrens TE , Woolrich MW , Smith SM , 2012 FSL. NeuroImage 62 (2), 782–790.21979382

Jeurissen B , Tournier J-D , Dhollander T , Connelly A , Sijbers J , 2014 Multi-tissue constrained spherical deconvolution for improved analysis of multi-shell diffusion MRI data. NeuroImage 103, 411–426.25109526

Jianu R , Demiralp C , Laidlaw D , 2009 Exploring 3D DTI fiber tracts with linked 2D representations. IEEE transactions on visualization and computer graphics 15 (6), 1449–1456.19834220

Jin Y , Shi Y , Zhan L , Gutman BA , de Zubicaray GI , McMahon KL , Wright MJ , Toga AW , Thompson PM , 2014 Automatic clustering of white matter fibers in brain diffusion MRI with an application to genetics. NeuroImage 100, 75–90.24821529

Kammen A , Law M , Tjan BS , Toga AW , Shi Y , 2016 Automated retinofugal visual pathway reconstruction with multi-shell HARDI and FOD-based analysis. NeuroImage 125, 767–779.26551261

Kazemi K , Moghaddam HA , Grebe R , Gondry-Jouet C , Wallois F , 2007 A neonatal atlas template for spatial normalization of whole-brain magnetic resonance images of newborns: preliminary results. NeuroImage 37 (2), 463–473.17560795

Kumar K , Desrosiers C , Siddiqi K , Colliot O , Toews M , 2017 Fiberprint: A subject fingerprint based on sparse code pooling for white matter fiber analysis. NeuroImage 158, 242–259.28684331

Labra N , Guevara P , Duclap D , Houenou J , Poupon C , Mangin J-F , Figueroa M , 2017 Fast automatic segmentation of white matter streamlines based on a multi-subject bundle atlas. Neuroinformatics 15 (1), 71–86.27722821

Lawes INC , Barrick TR , Murugam V , Spierings N , Evans DR , Song M , Clark CA , 2008 Atlas-based segmentation of white matter tracts of the human brain using diffusion tensor tractography and comparison with classical dissection. NeuroImage 39 (1), 62–79.17919935

Lebel C , Gee M , Camicioli R , Wieler M , Martin W , Beaulieu C , 2012 Diffusion tensor imaging of white matter tract evolution over the lifespan. NeuroImage 60 (1), 340–352.22178809

Lefranc S , Roca P , Perrot M , Poupon C , Le Bihan D , Mangin J-F , Rivière D , 2016 Groupwise connectivity-based parcellation of the whole human cortical surface using watershed-driven dimension reduction. Medical Image Analysis 30, 11–29.26849421

Li H , Xue Z , Guo L , Liu T , Hunter J , Wong ST , 2010 A hybrid approach to automatic clustering of white matter fibers. NeuroImage 49 (2), 1249–1258.19683061

Liao R , Ning L , Chen Z , Rigolo L , Gong S , Pasternak O , Golby AJ , Rathi Y , O'Donnell LJ , 2017 Performance of unscented Kalman filter tractography in edema: Analysis of the two-tensor model. NeuroImage: Clinical 15, 819–831.

Maddah M , Mewes AU , Haker S , Grimson WEL , Warfield SK , 2005 Automated atlas-based clustering of white matter fiber tracts from DTMRI. In: International Conference on Medical Image Computing and Computer-Assisted Intervention (MICCAI) Springer, pp. 188–195.

Maier-Hein KH , Neher PF , Houde J-C , Ct M-A , Garyfallidis E , Zhong J , Chamberland M , Yeh F-C , Lin Y-C , Ji Q , Reddick WE , Glass JO , Chen DQ , Feng Y , Gao C , Wu Y , Ma J , Renjie H , Li Q , Westin C-F , Deslauriers-Gauthier S , Gonzlez JOO , Paquette M , St-Jean S , Girard G , Rheault F , Sidhu J , Tax CMW , Guo F , Mesri HY , Dvid S , Froeling M , Heemskerk AM , Leemans A , Bor A , Pinsard B , Bedetti C , Desrosiers M , Brambati S , Doyon J , Sarica A , Vasta R , Cerasa A , Quattrone A , Yeatman J , Khan AR , Hodges W , Alexander S , Romascano D , Barakovic M , Aura A , Esteban O , Lemkaddem A , Thiran J-P , Cetingul HE , Odry BL , Mailhe B , Nadar MS , Pizzagalli F , Prasad G , Villalon-Reina JE , Galvis J , Thompson PM , Requejo FDS , Laguna PL , Lacerda LM , Barrett R , Dell'Acqua F , Catani M , Petit L , Caruyer E , Daducci A , Dyrby TB , Holland-Letz T , Hilgetag CC , Stieltjes B , Descoteaux M , 2016 Tractography-based connectomes are dominated by false-positive connections. bioRxiv, 084137.

Maier-Hein KH , Neher PF , Houde J-C , Ct M-A , Garyfallidis E , Zhong J , Chamberland M , Yeh F-C , Lin Y-C , Ji Q , Reddick WE , Glass JO , Chen DQ , Feng Y , Gao C , Wu Y , Ma J , Renjie H , Li Q , Westin C-F , Deslauriers-Gauthier S , Gonzlez JOO , Paquette M , St-Jean S , Girard G , Rheault F , Sidhu J , Tax CMW , Guo F , Mesri HY , Dvid S , Froeling M , Heemskerk AM , Leemans A , Bor A , Pinsard B , Bedetti C , Desrosiers M , Brambati S , Doyon J , Sarica A , Vasta R , Cerasa A , Quattrone A , Yeatman J , Khan AR , Hodges W , Alexander S , Romascano D , Barakovic M , Aura A , Esteban O , Lemkaddem A , Thiran J-P , Cetingul HE , Odry BL , Mailhe B , Nadar MS , Pizzagalli F , Prasad G , Villalon-Reina JE , Galvis J , Thompson PM , Requejo FDS , Laguna PL , Lacerda LM , Barrett R , Dell'Acqua F , Catani M , Petit L , Caruyer E , Daducci A , Dyrby TB , Holland-Letz T , Hilgetag CC , Stieltjes B , Descoteaux M , 2017 The challenge of mapping the human connectome based on diffusion tractography. Nature communications 8 (1), 1349.

Makris N , Meyer JW , Bates JF , Yeterian EH , Kennedy DN , Caviness VS , 1999 MRI-based topographic parcellation of human cerebral white matter and nuclei: II. rationale and applications with systematics of cerebral connectivity. NeuroImage 9 (1), 18–45.9918726

Makropoulos A , Counsell SJ , Rueckert D , 2017a A review on automatic fetal and neonatal brain MRI segmentation. NeuroImage, in press.

Makropoulos A , Robinson EC , Schuh A , Wright R , Fitzgibbon S , Bozek J , Counsell SJ , Steinweg J , Passerat-Palmbach J , Lenz G , Mortari F , Tenev T , Duff EP , Bastiani M , Cordero-Grande L , Hughes E , Tusor N , Tournier J-D , Hutter J , Price AN , Murgasova M , Kelly C , Rutherford MA , Smith SM , Edwards AD , Hajnal JV , Jenkinson M , Rueckert D , 2017b The Developing Human Connectome Project: a minimal processing pipeline for neonatal cortical surface reconstruction. bioRxiv, 125526.

Malcolm JG , Shenton ME , Rathi Y , 2010 Filtered multitensor tractography. IEEE Transactions on Medical Imaging 29 (9), 1664–1675.20805043

Marek K , Jennings D , Lasch S , Siderowf A , Tanner C , Simuni T , Coffey C , Kieburtz K , Flagg E , Chowdhury S , Poewe W , Mollenhauer B , Klinik P-E , Sherer T , Frasier M , Meunier C , Rudolph A , Casaceli C , Seibyl J , Mendick S , Schuff N , Zhang Y , Toga A , Crawford K , Ansbach A , Blasio PD , Piovella M , Trojanowski J , Shaw L , Singleton A , Hawkins K , Eberling J , Brooks D , Russell D , Leary L , Factor S , Sommerfeld B , Hogarth P , Pighetti E , Williams K , Standaert D , Guthrie S , Hauser R , Delgado H , Jankovic J , Hunter C , Stern M , Tran B , Leverenz J , Baca M , Frank S , Thomas C-A , Richard I , Deeley C , Rees L , Sprenger F , Lang E , Shill H , Obradov S , Fernandez H , Winters A , Berg D , Gauss K , Galasko D , Fontaine D , Mari Z , Gerstenhaber M , Brooks D , Malloy S , Barone P , Longo K , Comery T , Ravina B , Grachev I , Gallagher K , Collins M , Widnell KL , Ostrowizki S , Fontoura P , Ho T , Luthman J , van der Brug M , Reith AD , Taylor P , 2011 The parkinson progression marker initiative (PPMI). Progress in Neurobiology 95 (4), 629–635.21930184

Mazziotta J , Toga A , Evans A , Fox P , Lancaster J , Zilles K , Woods R , Paus T , Simpson G , Pike B , Holmes C , Collins L , Thompson P , MacDonald D , Iacoboni M , Schormann T , Amunts K , Palomero-Gallagher N , Geyer S , Parsons L , Narr K , Kabani N , Goualher GL , Boomsma D , Cannon T , Kawashima R , Mazoyer B , 2001 A probabilistic atlas and reference system for the human brain: International Consortium for Brain Mapping (ICBM). Philosophical Transactions of the Royal Society of London B: Biological Sciences 356 (1412), 1293–1322.11545704

Mirzaalian H , Ning L , Savadjiev P , Pasternak O , Bouix S , Michailovich O , Grant G , Marx C , Morey R , Flashman L , George M , McAllister T , Andaluz N , Shutter L , Coimbra R , Zafonte

R , Coleman M , Kubicki M , Westin C-F , Stein M , Shenton M , Rathi Y , 2016 Inter-site and inter-scanner diffusion MRI data harmonization. NeuroImage 135, 311–323.27138209

Moberts B , Vilanova A , Van Wijk JJ , 2005 Evaluation of fiber clustering methods for diffusion tensor imaging In: VIS 05. IEEE Visualization. IEEE, pp. 65–72.

Mori S , Oishi K , Faria AV , 2009 White matter atlases based on diffusion tensor imaging. Current Opinion in Neurology 22 (4), 362369.

Mori S , van Zijl P , 2002 Fiber tracking: principles and strategies–a technical review. NMR in Biomedicine 15 (7–8), 468–480.12489096

Nimsky C , Ganslandt O , Merhof D , Sorensen AG , Fahlbusch R , 2006 Intraoperative visualization of the pyramidal tract by diffusion-tensor-imaging-based fiber tracking. NeuroImage 30 (4), 1219–1229.16364659

Ning L , Laun F , Gur Y , DiBella EV , Deslauriers-Gauthier S , Megherbi T , Ghosh A , Zucchelli M , Menegaz G , Fick R , St-Jean S , Paquette M , Aranda R , Descoteaux M , Deriche R , O'Donnell LJ , Rathi Y , 2015 Sparse reconstruction challenge for diffusion MRI: Validation on a physical phantom to determine which acquisition scheme and analysis method to use? Medical Image Analysis 26 (1), 316–331.26606457

Norton I , Essayed WI , Zhang F , Pujol S , Yarmarkovich A , Golby AJ , Kindlmann G , Wasserman D , Estepar RSJ , Rathi Y , Pieper S , Kikinis R , Johnson HJ , Westin C-F , O'Donnell LJ , 2017 SlicerDMRI: Open source diffusion MRI software for brain cancer research. Cancer Research 77 (21), e101–e103.29092950

O'Donnell LJ , Kubicki M , Shenton ME , Dreusicke MH , Grimson WEL , Westin C-F , 2006 A method for clustering white matter fiber tracts. American Journal of Neuroradiology 27 (5), 1032–1036.16687538

O'Donnell LJ , Suter Y , Rigolo L , Kahali P , Zhang F , Norton I , Albi A , Olubiyi O , Meola A , Essayed WI , Unadkat P , Ciris PA , Wells WM , Rathi Y , Westin C-F , Golby AJ , 2017 Automated white matter fiber tract identification in patients with brain tumors. NeuroImage: Clinical 13, 138–153.27981029

O'Donnell LJ , Wells WM , Golby AJ , Westin C-F , 2012 Unbiased groupwise registration of white matter tractography. In: International Conference on Medical Image Computing and Computer-Assisted Intervention (MICCAI) Springer, pp. 123–130.

O'Donnell LJ , Westin C-F , 2007 Automatic tractography segmentation using a high-dimensional white matter atlas. IEEE Transactions on Medical Imaging 26 (11), 1562–1575.18041271

Oguz I , Farzinfar M , Matsui J , Budin F , Liu Z , Gerig G , Johnson H , Styner M , 2014 DTIPrep: quality control of diffusion-weighted images. Neuroinformatics 8, 4.

Oishi K , Zilles K , Amunts K , Faria A , Jiang H , Li X , Akhter K , Hua K , Woods R , Toga AW , et al., 2008 Human brain white matter atlas: identification and assignment of common anatomical structures in superficial white matter. Neuroimage 43 (3), 447–457.18692144

Pannek K , Scheck SM , Colditz PB , Boyd RN , Rose SE , 2014 Magnetic resonance diffusion tractography of the preterm infant brain: a systematic review. Developmental Medicine & Child Neurology 56 (2), 113–124.24102176

Pecheva D , Yushkevich P , Batalle D , Hughes E , Aljabar P , Wurie J , Hajnal JV , Edwards AD , Alexander DC , Counsell SJ , Zhang H , 2017 A tract-specific approach to assessing white matter in preterm infants. NeuroImage 157, 675–694.28457976

Piper RJ , Yoong MM , Kandasamy J , Chin RF , 2014 Application of diffusion tensor imaging and tractography of the optic radiation in anteriortemporal lobe resection for epilepsy: a systematic review. Clinical Neurology and Neurosurgery 124, 59–6525016240

Poldrack R , Congdon E , Triplett W , Gorgolewski K , Karlsgodt K , Mumford J , Sabb F , Freimer N , London E , Cannon T , Bilder R , 2016 A phenome-wide examination of neural and cognitive function. Scientific Data 3, 160110.27922632

Porro-Muñoz D , Olivetti E , Sharmin N , Nguyen TB , Garyfallidis E , Avesani P , 2015 Tractome: a visual data mining tool for brain connectivity analysis. Data Mining and Knowledge Discovery 29 (5), 1258–1279.

Prasad G , Joshi SH , Jahanshad N , Villalon-Reina J , Aganj I , Lenglet C , Sapiro G , McMahon KL , de Zubicaray GI , Martin NG , Wrights MJ , Toga AW , Thompson PM , 2014 Automatic

clustering and population analysis of white matter tracts using maximum density paths. NeuroImage 97, 284–295.24747738

Qazi AA , Radmanesh A , O'Donnell L , Kindlmann G , Peled S , Whalen S , Westin C-F , Golby AJ , 2009 Resolving crossings in the corticospinal tract by two-tensor streamline tractography: method and clinical assessment using fMRI. Neuroimage 47, T98–T106.18657622

Reddy CP , Rathi Y , 2016 Joint multi-fiber NODDI parameter estimation and tractography using the unscented information filter. Frontiers in Neuro-science 10, 166.

Roberts JA , Perry A , Roberts G , Mitchell PB , Breakspear M , 2017 Consistency-based thresholding of the human connectome. NeuroImage 145, 118–129.27666386

Román C , Guevara M , Valenzuela R , Figueroa M , Houenou J , Duclap D , Poupon C , Mangin J-F , Guevara P , 2017 Clustering of whole-brain white matter short association bundles using HARDI data. Frontiers in Neuroinformatics 11, 73.29311886

Ros C , Güllmar D , Stenzel M , Mentzel H-J , Reichenbach JR , 2013 Atlas-guided cluster analysis of large tractography datasets. PloS one 8 (12), e83847.24386292

Schmahmann JD , 1996 From movement to thought: anatomic substrates of the cerebellar contribution to cognitive processing. Human Brain Mapping 4 (3), 174–198.20408197

Seo J , Jang S , 2013 different characteristics of the corticospinal tract according to the cerebral origin: DTI study. American Journal of Neuroradiology 34 (7), 1359–1363.23370470

Shany E , Inder TE , Goshen S , Lee I , Neil JJ , Smyser CD , Doyle LW , Anderson PJ , Shimony JS , 2017 Diffusion tensor tractography of the cerebellar peduncles in prematurely born 7-year-old children. The Cerebellum 16 (2), 314–325.27255706

Shi F , Yap P-T , Wu G , Jia H , Gilmore JH , Lin W , Shen D , 2011 Infant brain atlases from neonates to 1-and 2-year-olds. PloS one 6 (4), e18746.21533194

Siless V , Chang K , Fischl B , Yendiki A , 2018 Anatomicuts: Hierarchical clustering of tractography streamlines based on anatomical similarity. NeuroImage 166, 32–45.29100937

Sotiropoulos SN , Zalesky A , 2017 Building connectomes using diffusion MRI: Why, how and but. NMR in Biomedicine.

Sporns O , Tononi G , Kötter R , 2005 The human connectome: a structural description of the human brain. PLoS Computational Biology 1 (4), e42.16201007

Suarez RO , Commowick O , Prabhu SP , Warfield SK , 2012 Automated delineation of white matter fiber tracts with a multiple region-of-interest approach. NeuroImage 59 (4), 3690–3700.22155046

Sydnor VJ , Rivas-Grajales AM , Lyall AE , Zhang F , Bouix S , Karmacharya S , Shenton ME , Westin C-F , Makris N , Wassermann D , O'Donnell LJ , Kubicki M , 2018 A comparison of three fiber tract delineation methods and their impact on white matter analysis. NeuroImage, in press.

Tak HJ , Kim JH , Son SM , 2016 Developmental process of the arcuate fasciculus from infancy to adolescence: a diffusion tensor imaging study. Neural Regeneration Research 11 (6), 937.27482222

Tang Y , Sun W , Toga AW , Ringman JM , Shi Y , 2018 A probabilistic atlas of human brainstem pathways based on connectome imaging data. NeuroImage 169, 227–239.29253653

Tax CM , Chamberland M , van Stralen M , Viergever MA , Whittingstall K , Fortin D , Descoteaux M , Leemans A , 2015 Seeing more by showing less: Orientation-dependent transparency rendering for fiber tractography visualization. PloS one 10 (10), e0139434.26444010

Thomas C , Frank QY , Irfanoglu MO , Modi P , Saleem KS , Leopold DA , Pierpaoli C , 2014 Anatomical accuracy of brain connections derived from diffusion MRI tractography is inherently limited. Proceedings of the National Academy of Sciences 111 (46), 16574–16579.

Tunç B , Parker WA , Ingalhalikar M , Verma R , 2014 Automated tract extraction via atlas based adaptive clustering. NeuroImage 102, 596–607.25134977

Tunç B , Smith AR , Wasserman D , Pennec X , Wells WM , Verma R , Pohl KM , 2013 Multinomial probabilistic fiber representation for connectivity driven clustering In: Information Processing in Medical Imaging (IPMI). Vol. 7917 Springer, pp. 730–741.

Van Baarsen K , Kleinnijenhuis M , Jbabdi S , Sotiropoulos SN , Grotenhuis J , van Walsum A. v. C. , 2016 A probabilistic atlas of the cerebellar white matter. NeuroImage 124, 724–732.26385011

Van Essen DC , Smith SM , et al., 2013 The WU-Minn human connectome project: an overview. NeuroImage 80, 62–79.23684880

Varentsova A , Zhang S , Arfanakis K , 2014 Development of a high angular resolution diffusion imaging human brain template. NeuroImage 91, 177–186.24440528

Verhoeven JS , Sage CA , Leemans A , Van Hecke W , Callaert D , Peeters R , De Cock P , Lagae L , Sunaert S , 2010 Construction of a stereotaxic DTI atlas with full diffusion tensor information for studying white matter maturation from childhood to adolescence using tractography-based segmentations. Human Brain Mapping 31 (3), 470–486.19957267

Visser E , Nijhuis EH , Buitelaar JK , Zwiers MP , 2011 Partition-based mass clustering of tractography streamlines. NeuroImage 54 (1), 303–312.20673849

Wakana S , Caprihan A , Panzenboeck MM , Fallon JH , Perry M , Gollub RL , Hua K , Zhang J , Jiang H , Dubey P , Blitz A , Zijl P , Mori S , 2007 Reproducibility of quantitative tractography methods applied to cerebral white matter. NeuroImage 36 (3), 630–644.17481925

Wang Q , Yap P-T , Wu G , Shen D , 2013 Application of neuroanatomical features to tractography clustering. Human Brain Mapping 34 (9), 2089–2102.22461221

Wassermann D , Bloy L , Kanterakis E , Verma R , Deriche R , 2010 Unsupervised white matter fiber clustering and tract probability map generation: Applications of a gaussian process framework for white matter fibers. NeuroImage 51 (1), 228–241.20079439

Wassermann D , Makris N , Rathi Y , Shenton M , Kikinis R , Kubicki M , Westin C-F , 2016 The white matter query language: a novel approach for describing human white matter anatomy. Brain Structure and Function 221 (9), 4705–4721.26754839

Westin C-F , Maier SE , Mamata H , Nabavi A , Jolesz FA , Kikinis R , 2002 Processing and visualization for diffusion tensor MRI. Medical Image Analysis 6 (2), 93–108.12044998

Wu C-H , Hwang T-J , Chen Y-J , Hsu Y-C , Lo Y-C , Liu C-M , Hwu H-G , Liu C-C , Hsieh MH , Chien YL , Chen C-M , Tseng W-YI , 2015 Altered integrity of the right arcuate fasciculus as a trait marker of schizophrenia: A sibling study using tractography-based analysis of the whole brain. Human Brain Mapping 36 (3), 1065–1076.25366810

Wu Y , Zhang F , Makris N , Ning Y , Norton I , She S , Peng H , Rathi Y , Feng Y , Wu H , O'Donnell LJ , 2018 Investigation into local white matter abnormality in emotional processing and sensorimotor areas using an automatically annotated fiber clustering in major depressive disorder. NeuroImage, in press.

Xia Y , Turken U , Whitfield-Gabrieli SL , Gabrieli JD , 2005 Knowledge-based classification of neuronal fibers in entire brain. In: International Conference on Medical Image Computing and Computer-Assisted Intervention (MICCAI) Springer, pp. 205–212.

Yamada K , Sakai K , Akazawa K , Yuen S , Nishimura T , 2009 MR tractography: a review of its clinical applications. Magnetic Resonance in Medical Sciences 8 (4), 165–174.20035125

Yeh F-C , Badre D , Verstynen T , 2016 Connectometry: A statistical approach harnessing the analytical potential of the local connectome. NeuroImage 125, 162–171.26499808

Yeh F-C , Panesar S , Fernandes D , Meola A , Yoshino M , Fernandez-Miranda JC , Vettel JM , Verstynen T , 2018 Population-averaged atlas of the macroscale human structural connectome and its network topology. NeuroImage 178, 57–68.29758339

Yendiki A , Panneck P , Srinivasan P , Stevens A , Zllei L , Augustinack J , Wang R , Salat D , Ehrlich S , Behrens T , Jbabdi S , Gollub R , Fischl B , 2011 Automated probabilistic reconstruction of white-matter pathways in health and disease using an atlas of the underlying anatomy. Frontiers in Neuroinformatics 5 (23), 12–23.21863139

Yeo SS , Jang SH , Son SM , 2014 The different maturation of the corticospinal tract and corticoreticular pathway in normal brain development: diffusion tensor imaging study. Frontiers in Human Neuroscience 8, 573.25309378

Yoo SW , Guevara P , Jeong Y , Yoo K , Shin JS , Mangin J-F , Seong J-K , 2015 An example-based multi-atlas approach to automatic labeling of white matter tracts. PloS one 10 (7), e0133337.26225419

Zalesky A , Cocchi L , Fornito A , Murray MM , Bullmore E , 2012 Connectivity differences in brain networks. NeuroImage 60 (2), 1055–1062.22273567

Zhang F , Kahali P , Suter Y , Norton I , Rigolo L , Savadjiev P , Song Y , Rathi Y , Cai W , Wells WM , Golby AJ , O'Donnell LJ , 2017a Automated connectivity-based groupwise cortical atlas generation: Application to data of neurosurgical patients with brain tumors for cortical parcellation prediction. In: IEEE International Symposium on Biomedical Imaging (ISBI) IEEE, pp. 774–777.

Zhang F , Norton I , Cai W , Song Y , Wells WM , O'Donnell LJ , 2017b Comparison between two white matter segmentation strategies: an investigation into white matter segmentation consistency. In: IEEE International Symposium on Biomedical Imaging (ISBI) IEEE, pp. 796–799.

Zhang F , Savadjiev P , Cai W , Song Y , Rathi Y , Tunç B , Parker D , Kapur T , Schultz RT , Makris N , Verma R , O'Donnell LJ , 2018a Whole brain white matter connectivity analysis using machine learning: An application to autism. NeuroImage 172, 826–837.29079524

Zhang F , Wu W , Ning L , McAnulty G , Waber D , Gagoski B , Sarill K , Hamoda H , Song Y , Cai W , Rathi Y , O'Donnell LJ , 2018b Suprathreshold fiber cluster statistics: leveraging white matter geometry to enhance tractography statistical analysis. NeuroImage 171, 341–354.29337279

Zhang W , Olivi A , Hertig SJ , Van Zijl P , Mori S , 2008 Automated fiber tracking of human brain white matter using diffusion tensor imaging. NeuroImage 42 (2), 771–777.18554930

Zhang Y , Park SH , Pohl KM , 2016 Joint data harmonization and group cardinality constrained classification. In: International Conference on Medical Image Computing and Computer-Assisted Intervention (MICCAI) Springer, pp. 282–290.

Zhang Y , Zhang J , Oishi K , Faria AV , Jiang H , Li X , Akhter K , Rosa-Neto P , Pike GB , Evans A , Toga AW , Woods R , Mazziotta JC , Miller MI , van Zijl PC , Mori S , 2010 Atlas-guided tract reconstruction for automated and comprehensive examination of the white matter anatomy. NeuroImage 52 (4), 1289–1301.20570617

Ziyan U , Sabuncu MR , Grimson WEL , Westin C-F , 2009 Consistency clustering: a robust algorithm for group-wise registration, segmentation and automatic atlas construction in diffusion MRI. International Journal of Computer Vision 85 (3), 279–290.20442792

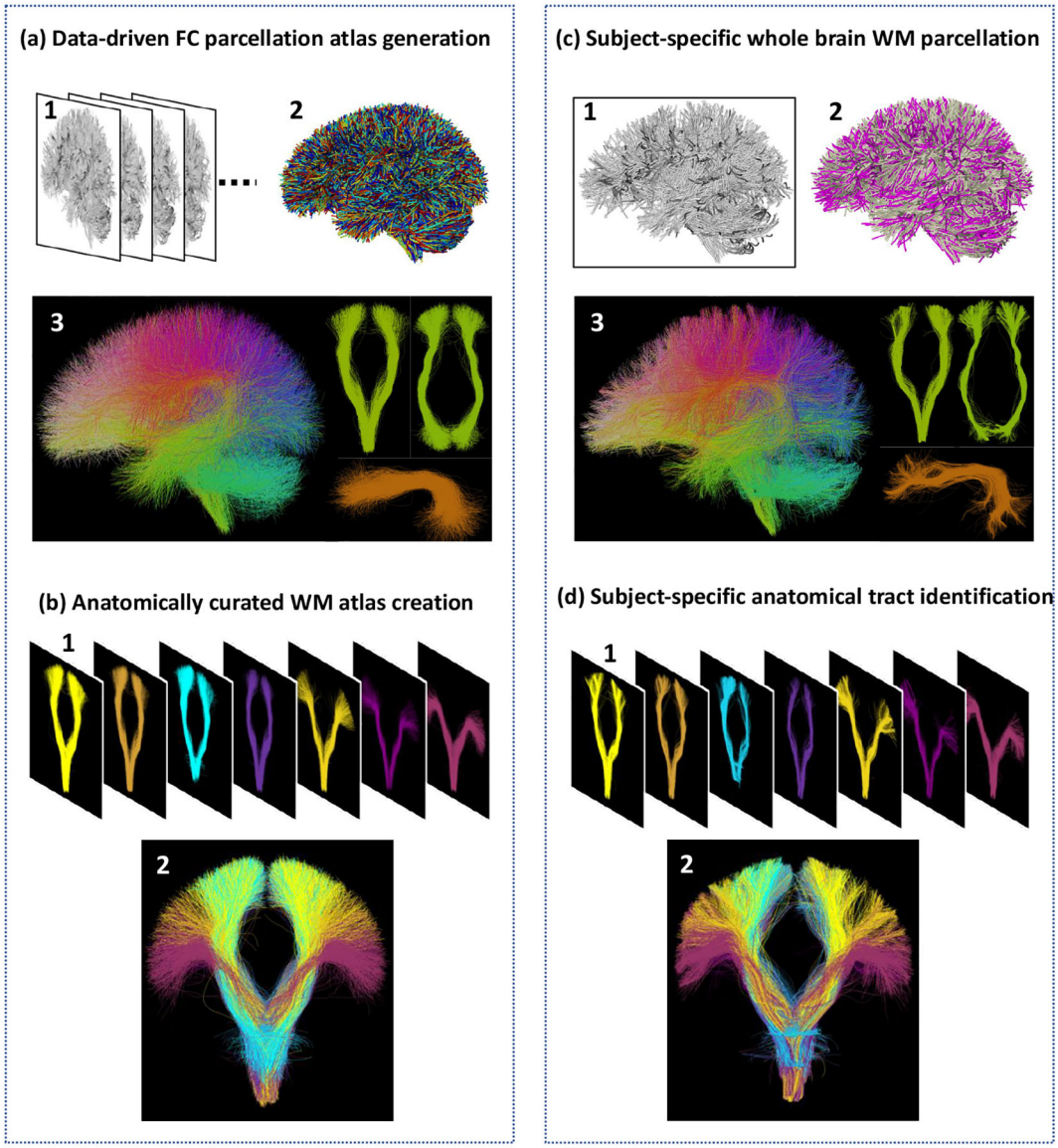

Figure 1:

Method overview. Sub-figure (a) shows the data-driven fiber clustering atlas generation process. Given the input tractography (a.1) from the 100 atlas subjects, a groupwise whole brain tractography registration for simultaneous joint alignment of tractography across all subjects (fibers from different subjects colored differently) is conducted (a.2). Spectral clustering is performed to generate the fiber clustering atlas (each cluster has a unique color as shown in a.3). Three example individual fiber clusters are displayed. Sub-figure (b) displays the corticospinal tract (CST) in the atlas, as curated by an expert neuroanatomist. Several example clusters belonging to the CST are displayed (b.1), where each cluster represents a specific subdivision of the whole CST (b.2). Sub-figure (c) demonstrates whole brain white matter tract parcellation for a new subject. The new subject's tractography (c.1) is first registered to the atlas tractography (colored in pink in c.2). Fiber clustering of the aligned tractography is then conducted according to the fiber clustering atlas for whole brain

white matter tract parcellation (c.3). Sub-figure (d) illustrates the subject-specific anatomical tract identification. Identification of the CST (d.2) in the new subject is conducted by finding the corresponding subject-specific clusters (d.1) to those annotated as the CST in the atlas.

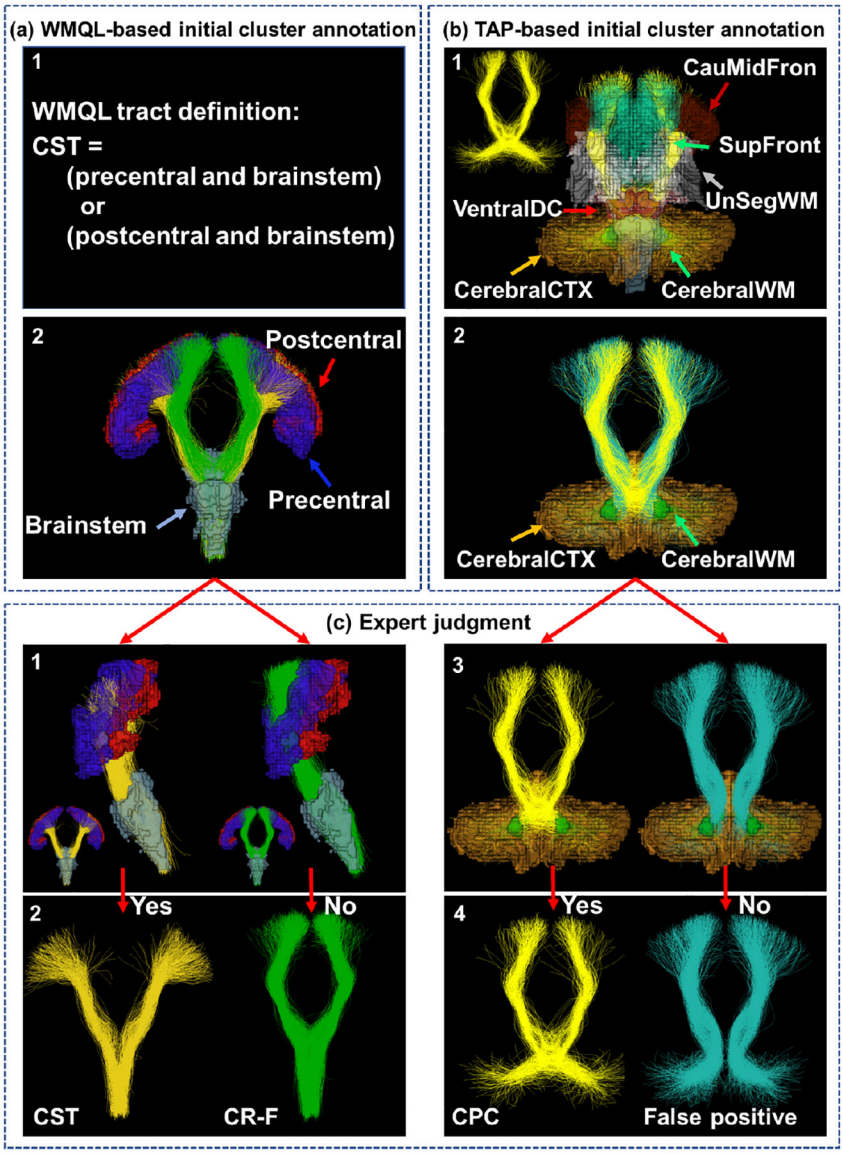

Figure 2:

Overview of the fiber cluster anatomical annotation method, including two initial annotation computation steps, followed by expert judgment. Sub-figure (a) shows the initial cluster annotation using White Matter Query Language (WMQL) that provides anatomical definitions of fiber tracts based on their intersected Freesurfer regions. The corticospinal tract (CST) is selected for illustration. Any fiber clusters that have fibers meeting the WMQL CST definition (a.1) are initially identified to belong to CST. Two example clusters (a.2) are displayed. Sub-figure (b) shows the initial cluster annotation using tract anatomical profile (TAP) that is defined as a set of Freesurfer regions through which a cluster passed. The TAP of the example yellow cluster contains six Freesurfer regions (b.1). TAP-based initial annotation for the cerebellar tract is used for illustration. Any fiber clusters that have TAP containing the cerebral-cortex or cerebral-white-matter Freesurfer regions are initially identified to belong to the cerebellar tract. Two example clusters are displayed (b.2). After

the initial cluster annotation using the above two steps, expert judgment is performed for a final cluster annotation, as illustrated in sub-figure (c). For the two potentially CST clusters (c.1 and c.2), the yellow cluster is accepted; however, the green cluster is rejected because most of its fibers do not touch the precentral or postcentral gyri, and a corrected annotation of the corona-radiata-frontal (CR-F) tract is provided. For the two clusters potentially belonging to the cerebellar tract (c.3 and c.4), the yellow cluster is accepted and an annotation of a sub-category, i.e. the cortico-ponto-cerebellar (CPC) tract, is provided; however, the green cluster is rejected because the white matter connections between the cerebellum and the cortex should cross the hemispheres, and thus this cluster is categorized as a false positive tract.

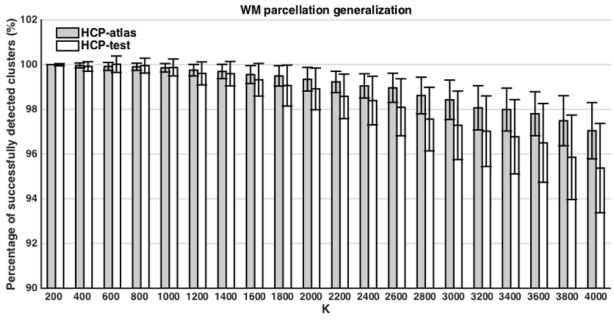

(a) White matter parcellation generalization (WMPG)

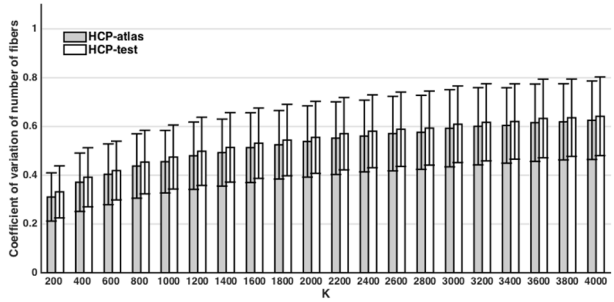

(b) Inter-subject parcellation variability (ISPV)

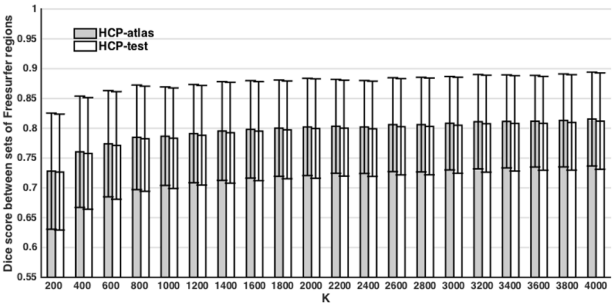

(c) Tract anatomical profile coherence (TAPC)

Figure 3:

Quantitative evaluations for whole brain white matter parcellations at different scales (k = 200 to 4000) using the two HCP datasets. At each parcellation scale, WMPG (a), ISPV (b) and TAPC (c) were computed, as described in Section 2.5. WMPG was used to measure if all fiber clusters could be generally detected in the population. ISPV was computed to measure if the number of fibers in the corresponding clusters were similar. TAPC was used to measure if fibers within a cluster commonly passed through the same Freesurfer regions.

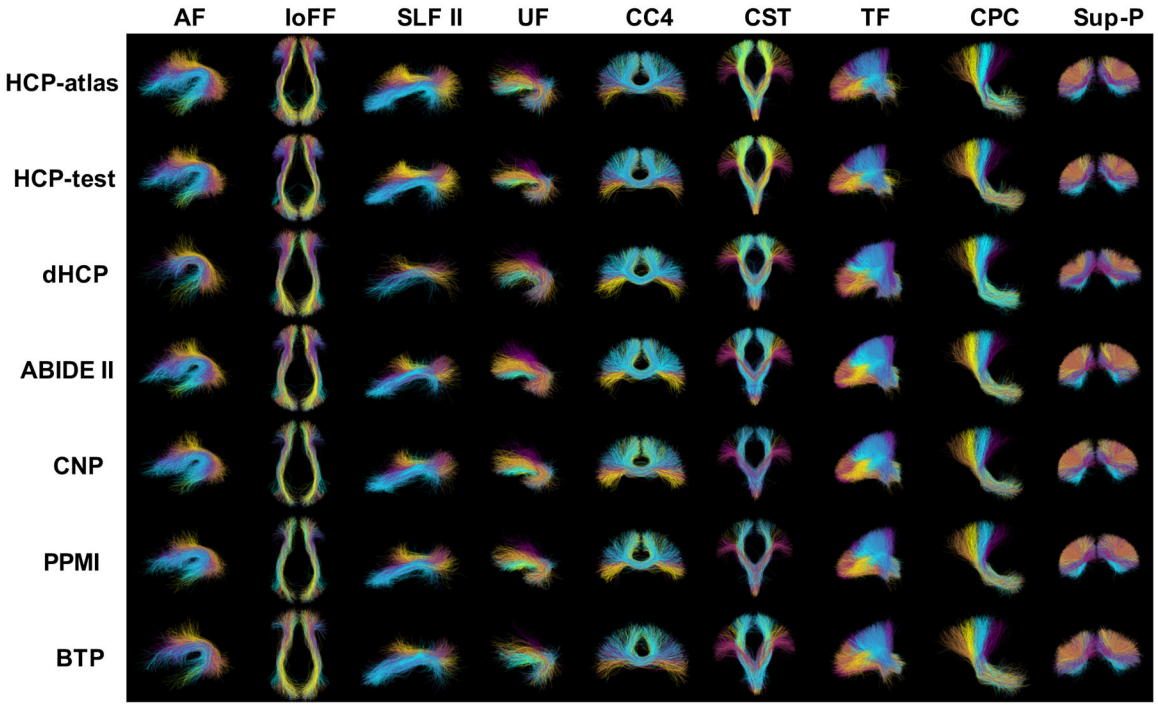

Figure 4:

Population-based visualizations for several example fiber tracts. For each tract, individual fiber clusters are displayed in different colors. For AF, SLF II, UF, TF and CPC, a left view is displayed; for IoFF, a superior view is displayed; for CC4, CST and Sup-P, a anterior view is displayed.

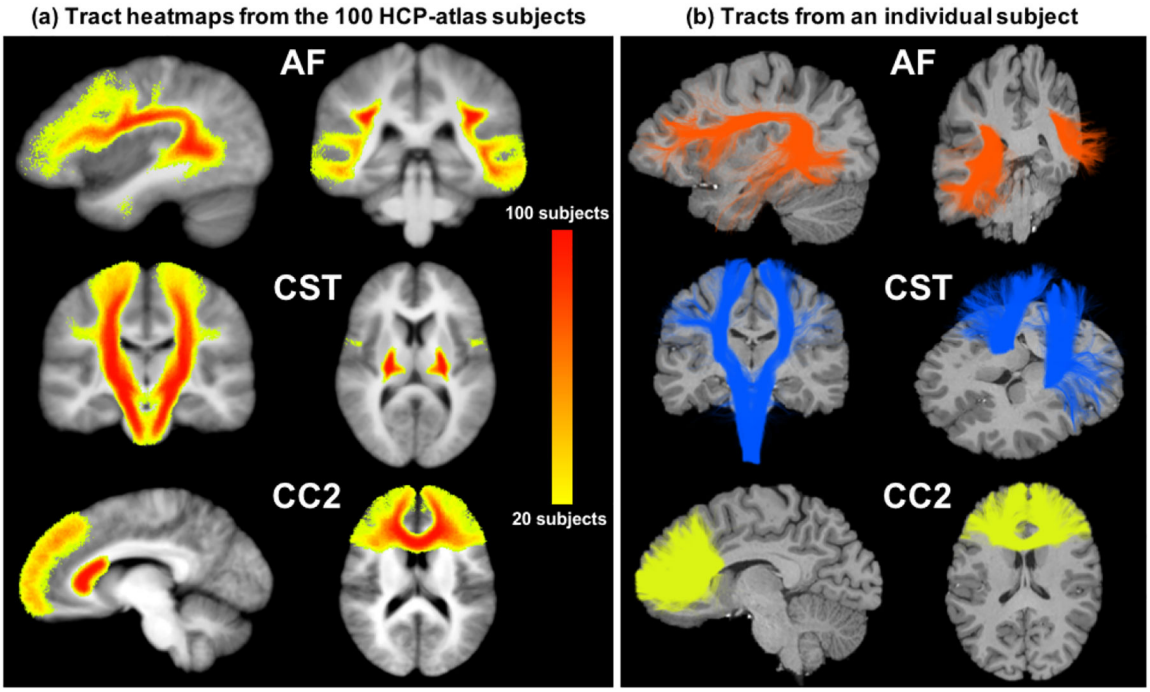

Figure 5:
(a) Voxel-based tract heatmaps of three example fiber tracts based on the 100 HCP-atlas subjects. The value of a voxel in the heatmaps represents the number of subjects that have fibers passing through the voxel. The background image is the population mean T1 image from all HCP-100 subjects (Section 2.2). (b) The corresponding tracts from one individual HCP-atlas subject, overlaid on the subject's T1 image.

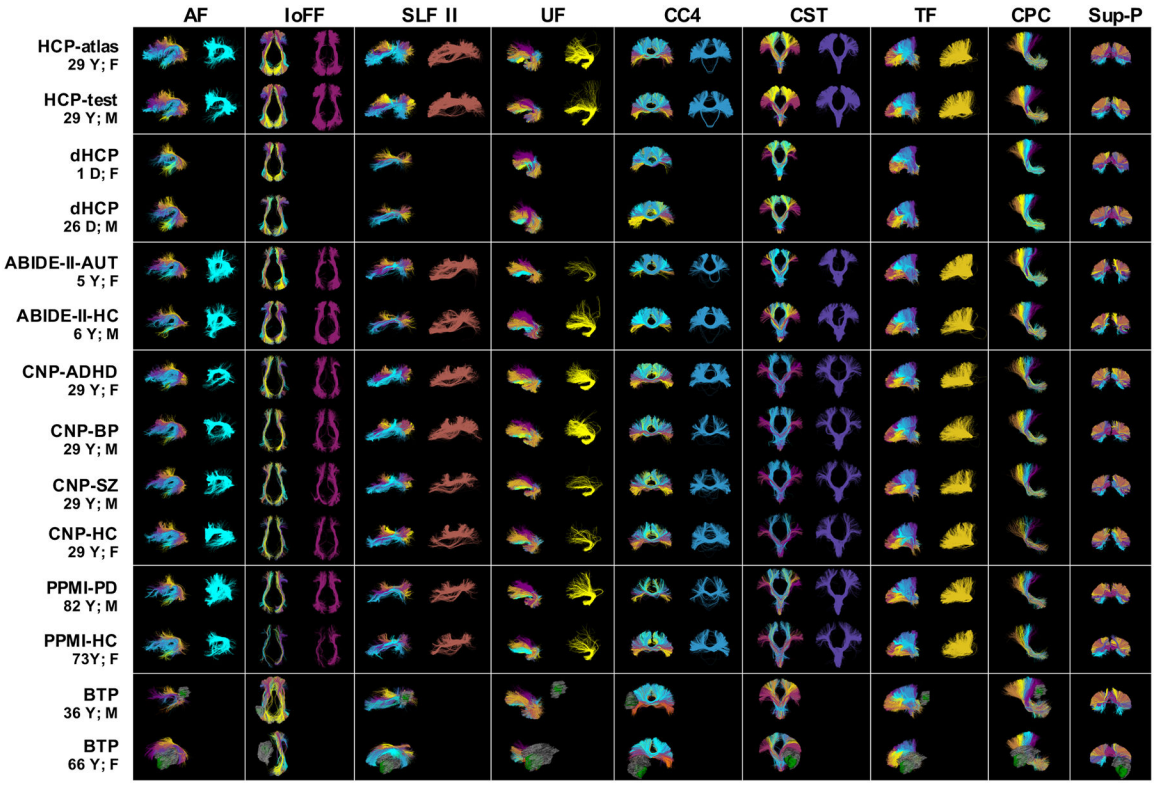

Figure 6:

Visualizations of example subject-specific fiber tracts identified using the proposed method (left) and the WMQL method (right). For the CPC and Sup-P tracts, only results from our method are displayed because there were not corresponding definitions in WMQL. Individuals from the multiple datasets under study were selected as follows. For each of the HCP-atlas and the HCP-test datasets, an adult who had a population mean age (29 years) was selected. For the dHCP dataset, the youngest (1 day) and the oldest (27 days) neonates were selected. For the ABIDE-II dataset, the youngest AUT (5.1 years) and healthy control (5.9 years) were selected. For the CNP dataset, four 29-year-old adults (same as the population mean age of the HCP-atlas subjects), respectively, from the ADHD, BP, SZ and healthy groups were selected. For the PPMI dataset, two individuals who had the highest ages in the PD and healthy groups (82 and 80 years, respectively) were selected. For the BTP dataset, tracts from two patients (36 and 66 years old) were selected. The tumor (green) and surrounding edema (gray) are visualized for each patient.

Table 1:

Summary of existing white matter atlases to describe the current state of the art. For each study, the number of tracts that are defined, the population used to create the atlas, the test population to perform subject-specific parcellation and if the atlas is publicly available are reported. We note that bilateral structures were considered as two separated tracts (e.g. left and right arcuate fasciculus tracts (AF)) when calculating the number of tracts.

Study	Tracts	Atlas population	Parcellation test population	Publicly available
Voxel-based white matter atlases				
Hua et al. (2008)	20 deep WM tracts	28 healthy (29±7.9Y, 11F/17M)	1 multiple sclerosis patient (32Y, M)	Yes †
Hagler et al. (2009)	23 deep WM tracts	21 healthy (21–52Y, 11F/10M) & 21 temporal lobe epilepsy patients (21—54Y)	Same as the atlas population	No
Bazin et al. (2011)	39 deep WM tracts	Not given	21 healthy (22–61Y, 10F/11M)	Yes *
de Schotten et al. (2011)	30 deep WM tracts	40 healthy (18–22Y, 20F/20M)	1 hemiplegia patient (68Y, F) & 1 chronic neglect patient (61Y, M)	Yes ‡
Yendiki et al. (2011)	18 deep WM tracts	33 healthy (42±10Y, 14F/19M) & 34 schizophrenia patients (37±10Y, 9F/25M)	Same as the atlas population	Yes §
Suarez et al. (2012)	11 deep WM tracts	20 healthy (17.8±1.1Y, 10F/10M)	Same as the atlas population	No
Ros et al. (2013)	16 deep WM tracts	15 healthy (randomly selected from the test population)	46 healthy (24F, 29±8.66Y; 22M, 29±9.99Y)	No
Van Baarsen et al. (2016)	6 cerebellar tracts	90 healthy (22–35Y)	Not applicable	Yes ‖
Akazawa et al. (2016)	24 deep WM tracts	11 term-born neonates (within 3 days of life, 7F/4M)	19 term-born and 30 preterm-born babies	No
Tang et al. (2018)	23 brainstem tracts	20 healthy (10F/10M)	Not applicable	Yes ††
Tract-based white matter atlases				
Maddah et al. (2005)	Not given	1 healthy	4 healthy	No
O'Donnell and Westin (2007)	19 deep WM tracts	10 subjects	5 subjects	No
Ziyan et al. (2009)	5 deep WM tracts	15 healthy (young)	Same as the atlas population	No
Guevara et al. (2012)	36 deep WM tracts, plus 94 superficial fiber parcels	12 healthy (adults)	20 healthy (adults)	Yes **
Jin et al. (2014)	17 deep WM tracts	5 healthy (randomly selected from the test population)	198 healthy (23.2±2.1Y)	No
Tunç et al. (2014)	11 deep WM tracts	4 healthy (31.25±4.2Y, M)	2 healthy (31.25±4.2 Y, M)	No
Yoo et al. (2015)	14 deep WM tracts	12 healthy (21±40Y, 12M)	Same as the atlas population	No
Labra et al. (2017)	26 deep WM tracts	4 healthy	Not given	Yes ‡‡
Guevara et al. (2017)	100 superficial fiber parcels	79 healthy (23.6±5.2Y, 32F/47M)	26 subjects	Yes ‡‡
Román et al. (2017)	93 superficial fiber parcels	74 healthy (23.6±5.2Y, 31F/43M)	78 subjects	Yes ‡‡
Yeh et al. (2018)	66 deep WM tracts, plus set of U-fibers	842 healthy (22–36Y, 470F/372M)	Not applicable	Yes §§

Study	Tracts	Atlas population	Parcellation test population	Publicly available
O'Donnell et al. (2017)	10 deep WM tracts	10 healthy (adult)	18 brain tumor patients (28—70Y)	No
Proposed	58 deep WM tracts, plus 198 superficial fiber parcels organized into 16 categories. Also includes potential false positive fibers, plus a whole brain WM parcellation into 800 parcels	100 healthy (22–36Y, 54F/46M)	584 subjects with multiple health conditions (1D—72Y, 253F/331M)	Yes[///]

[†] http://lbam.med.jhmi.edu;

[*] https://www.nitrc.org/projects/dots;

[‡] https://www.natbrainlab.co.uk/atlas-maps;

[§] https://surfer.nmr.mgh.harvard.edu/fswiki/Tracula;

[//] https://www.nitrc.org/projects/cer_wm_atlas/;

[††] https://www.nitrc.org/projects/brainstem_atlas;

[**] http://brainvisa.info/web/index.html;

[‡‡] http://neurospin.github.io/pyconnectomist;

[§§] http://brain.labsolver.org;

[///] https://dmri.slicer.org/atlases.

Table 2:

Demographics, dMRI acquisition, and the availability of Freesurfer segmentation of the datasets under study.

Dataset	# Sub	Age	Gender	Health/Disease	dMRI data	Freesurfer
HCP-atlas	100	22 to 36 years (29.1±3.7)	54 F 46 M	100 healthy	b=3000 s/mm^2 108 directions TE/TR=89/5520 ms resolution=1.25 mm^3	Yes
HCP-test	100	22 to 35 years (29.0±3.5)	54 F 46 M	100 healthy	b=3000 s/mm^2 108 directions TE/TR=89/5520 ms resolution=1.25 mm^3	Yes
dHCP	40	1 to 27 days (6.30±7.47)	15 F 25 M	40 healthy	b=400/1000/2600 s/mm^2 300 directions TE/TR=90/3800 ms resolution=1.5 mm^3	No
ABIDE-II	70	5 to 17 years (12.0±3.1)	6F 64 M	49 AUT 21 healthy	b=1000 s/mm^2 64 directions TE/TR=78/5200 ms resolution=3 mm^3	Yes
CNP	204	21 to 50 years (33.3±9.3)	112 F 153 M	41 ADHD 49 BD 50 SZ 125 healthy	b=1000 s/mm^2 64 directions TE/TR=93/9000 ms resolution=2 mm^3	Yes
PPMI	144	51 to 82 years (63.7±7.3)	51 F 93 M	102 PD 42 healthy	b=1000 s/mm^2 64 directions TE/TR=88/7600 ms resolution=2 mm^3	Yes
BTP	26	23 to 72 years (49.4±14.9)	15 F 11 M	26 brain tumor patients	b=2000 s/mm^2 31 directions TE/TR=98/12700 ms resolution=2.3 mm^3	No
Total subjects = 684 (100 subjects for atlas generation and 584 subjects for testing)						

Abbreviations: Dataset: HCP - Human Connectome Project; dHCP - Developing Human Connectome Project; ABIDE-II - Autism Brain Imaging Data Exchange II; CNP - Consortium for Neuropsychiatric Phenomics; PPMI - Parkinson's Progression Markers Initiative; BTP - Brain Tumor Patient. Gender: F - female; M - Male. Disease: AUT - autism; ADHD - attention-deficit/hyperactivity disorder; BP - bipolar disorder; SZ - schizoprenia; PD - Parkinson's disease.

Table 3:

Anatomical tracts annotated in the proposed white matter atlas. Except for the 7 corpus callosum (CC) tracts and the middle cerebellar peduncle (MCP) tract that cross the hemispheres (C), others are hemispheric (LR). Overall, there are 58 deep white matter fiber tracts from the association, cerebellar, commissural and projection tracts, and 16 superficial tract categories according to the brain lobes.

Tract category (tract #)	Tract name
Association tracts (24)	arcuate fasciculus (AF) – LR
	cingulum bundle (CB) – LR
	external capsule (EC) – LR
	extreme capsule (EmC) – LR
	inferior longitudinal fasciculus (ILF) – LR
	inferior occipito-frontal fasciculus (IoFF) – LR
	middle longitudinal fasciculus (MdLF) – LR
	posterior limb of internal capsule (PLIC) – LR
	superior longitudinal fasciculus I (SLF I) – LR
	superior longitudinal fasciculus II (SLF II) – LR
	superior longitudinal fasciculus II (SLF III) – LR
	uncinate fasciculus (UF) – LR
Cerebellar tracts (9)	cortico-ponto-cerebellar (CPC) – LR
	inferior cerebellar peduncle (ICP) – LR
	intracerebellar input and Purkinje tract (Intra-CBLM-I&P) – LR
	intracerebellar parallel tract (Intra-CBLM-PaT) – LR
	middle cerebellar peduncle (MCP) – C
Commissural tracts (7)	corpus callosum 1 (CC 1) – C
	corpus callosum 1 (CC 1) – C
	corpus callosum 2 (CC 2) – C
	corpus callosum 3 (CC 3) – C
	corpus callosum 4 (CC 4) – C
	corpus callosum 5 (CC 5) – C
	corpus callosum 6 (CC 6) – C
	corpus callosum 7 (CC 7) – C
Projection tracts (18)	corticospinal tract (CST) – LR
	corona-radiata-frontal (CR-F) (excluding the CST) – LR
	corona-radiata-parietal (CR-P) (excluding the CST) – LR
	striato-frontal (SF) – LR
	striato-occipital (SO) – LR
	striato-parietal (SP) – LR
	thalamo-frontal (TF) – LR
	thalamo-occipital (TO) – LR
	thalamo-parietal (TP) – LR

Tract category (tract #)	Tract name
Superficial tracts (16)	superficial-frontal (Sup-F) – LR
	superficial-frontal-parietal (Sup-FP) – LR
	superficial-occipital (Sup-O) – LR
	superficial-occipital-temporal (Sup-OT) – LR
	superficial-parietal (Sup-P) – LR
	superficial-parietal-occipital (Sup-PO) – LR
	superficial-parietal-temporal (Sup-PT) – LR
	superficial-temporal (Sup-T) – LR

Table 4:

White matter parcellation generalization evaluations on the testing datasets. For comparison, results from the two HCP datasets are listed.

Dataset	K = 800	K = 2000
HCP-atlas	99.906 ± 0.159	99.350 ± 0.531
HCP-test	99.759 ± 0.367	98.717 ± 1.025
dHCP	90.706 ± 5.482	76.196 ± 8.517
ABIDE-II-AUT	94.513 ± 2.222	87.177 ± 3.521
ABIDE-II-HC	95.685 ± 1.335	87.448 ± 2.487
CNP-ADHD	96.598 ± 1.756	90.735 ± 2.787
CNP-BP	96.786 ± 1.544	90.676 ± 2.313
CNP-SZ	96.306 ± 1.567	90.089 ± 2.553
CNP-HC	95.974 ± 1.368	89.593 ± 2.286
PPMI-PD	97.106 ± 1.235	91.148 ± 2.546
PPMI-HC	96.903 ± 1.264	90.330 ± 2.545
BTP	92.567 ± 6.010	81.427 ± 9.060

Table 5:

Inter-subject parcellation variability evaluations on the testing datasets. For com parison, results from the two HCP datasets are listed.

Dataset	K = 800	K = 2000
HCP-atlas	0.439 ± 0.136	0.550 ± 0.165
HCP-test	0.463 ± 0.150	0.578 ± 0.182
dHCP	0.844 ± 0.333	1.014 ± 0.350
ABIDE-II-AUT	0.713 ± 0.317	0.878 ± 0.344
ABIDE-II-HC	0.703 ± 0.314	0.848 ± 0.339
CNP-ADHD	0.588 ± 0.223	0.721 ± 0.252
CNP-BP	0.587 ± 0.240	0.719 ± 0.262
CNP-SZ	0.608 ± 0.256	0.746 ± 0.287
CNP-HC	0.605 ± 0.240	0.746 ± 0.266
PPMI-PD	0.601 ± 0.206	0.751 ± 0.246
PPMI-HC	0.611 ± 0.222	0.757 ± 0.256
BTP	0.800 ± 0.274	0.946 ± 0.301

Table 6:

Tract anatomical profile coherence evaluations on the testing datasets. For comparison, results from the two HCP datasets are listed. Due to the unavailability of the Freesurfer segmentations of the subjects in the dHCP and BTP datasets, their profile coherence measurements were not able to be computed.

Dataset	K = 800	K = 2000
HCP-atlas	0.785 ± 0.088	0.802 ± 0.082
HCP-test	0.782 ± 0.088	0.800 ± 0.083
dHCP	–	–
ABIDE-II-AUT	0.748 ± 0.094	0.763 ± 0.092
ABIDE-II-HC	0.755 ± 0.094	0.772 ± 0.092
CNP-ADHD	0.759 ± 0.095	0.777 ± 0.090
CNP-BP	0.760 ± 0.095	0.777 ± 0.091
CNP-SZ	0.757 ± 0.094	0.775 ± 0.090
CNP-HC	0.756 ± 0.095	0.774 ± 0.091
PPMI-PD	0.761 ± 0.094	0.777 ± 0.092
PPMI-HC	0.760 ± 0.095	0.776 ± 0.093
BTP	–	–

Table 7:

Quantitative comparisons of the tract identification results using the proposed method and the WMQL method, in terms of the white matter parcellation generalization (WMPG), the inter-subject parcellation variability (ISPV) and the tract anatomical profile coherence (TAPC). A high WMPG value indicates a high generalization of the atlas to subjects in each dataset; a low ISPV value represents a low parcellation variability and thus a high consistency across the subjects in each dataset; a high TAPC value suggests a high anatomical coherence of the fibers in each cluster. The comparisons were performed on all annotated hemispheric and commissural tracts, which were divided into three groups: 1) the 45 deep white tracts that both methods were able to identify (DT-45), 2) the 13 deep white tracts that were defined in our method but not in the WMQL method (DT-13), and 3) the 198 short and medium range superficial fiber tracts (ST-198) that were defined in our method.

		Proposed			WMQL		
	Tracts	**WMPG**	**ISPV**	**TAPC**	**WMPG**	**ISPV**	**TAPC**
HCP-atlas	DT-45	100.0 ± 0.0	0.264 ± 0.075	0.668 ± 0.075	100.0 ± 0.0	0.353 ± 0.117	0.696 ± 0.076
	DT-13	100.0 ± 0.0	0.368 ± 0.108	0.779 ± 0.102	–-	–	–
	ST-198	99.96 ± 0.14	0.488 ± 0.110	0.783 ± 0.062	–	–	–
HCP-test	DT-45	100.0 ± 0.0	0.280 ± 0.079	0.666 ± 0.075	100.0 ± 0.0	0.389 ± 0.172	0.697 ± 0.075
	DT-13	100.0 ± 0.0	0.356 ± 0.091	0.776 ± 0.104	–	–	–
	ST-198	99.85 ± 0.45	0.513 ± 0.119	0.781 ± 0.061	–	–	–
dHCP	DT-45	99.56 ± 1.03	0.533 ± 0.186	–	–	–	–
	DT-13	97.71 ± 7.55	0.625 ± 0.295	–	–	–	–
	ST-198	93.08 ± 7.55	0.919 ± 0.264	–	–	–	–
ABIDE-II-AUT	DT-45	99.95 ± 0.32	0.424 ± 0.156	0.639 ± 0.076	99.59 ± 0.87	0.532 ± 0.202	0.657 ± 0.079
	DT-13	99.49 ± 2.64	0.540 ± 0.231	0.726 ± 0.114	–	–	–
	ST-198	92.28 ± 4.48	0.845 ± 0.312	0.747 ± 0.067	–	–	–
ABIDE-II-HC	DT-45	100.0 ± 0.0	0.374 ± 0.168	0.644 ± 0.076	99.89 ± 0.48	0.457 ± 0.183	0.660 ± 0.082
	DT-13	100.0 ± 0.0	0.529 ± 0.199	0.727 ± 0.114	–	–	–
	ST-198	94.25 ± 2.60	0.853 ± 0.349	0.756 ± 0.069	–	–	–
CNP-ADHD	DT-45	100.0 ± 0.0	0.365 ± 0.127	0.629 ± 0.073	99.03 ± 1.31	0.492 ± 0.196	0.650 ± 0.088
	DT-13	100.0 ± 0.0	0.454 ± 0.141	0.745 ± 0.108	–	–	–
	ST-198	98.33 ± 1.95	0.634 ± 0.208	0.758 ± 0.062	–	–	–
CNP-BP	DT-45	100.0 ± 0.0	0.378 ± 0.141	0.631 ± 0.075	99.05 ± 1.83	0.498 ± 0.190	0.651 ± 0.090
	DT-13	99.78 ± 1.35	0.468 ± 0.147	0.743 ± 0.111	–	–	–
	ST-198	98.78 ± 1.46	0.623 ± 0.195	0.758 ± 0.063	–	–	–
CNP-SZ	DT-45	100.0 ± 0.0	0.377 ± 0.140	0.631 ± 0.072	99.52 ± 1.10	0.479 ± 0.178	0.651 ± 0.088
	DT-13	99.91 ± 0.88	0.477 ± 0.102	0.743 ± 0.112	–	–	–
	ST-198	98.33 ± 1.73	0.640 ± 0.205	0.756 ± 0.062	–	–	–
CNP-HC	DT-45	100.0 ± 0.0	0.371 ± 0.126	0.626 ± 0.072	99.67 ± 1.02	0.488 ± 0.179	0.647 ± 0.089
	DT-13	100.0 ± 0.0	0.462 ± 0.109	0.741 ± 0.104	–	–	–
	ST-198	98.55 ± 1.12	0.630 ± 0.185	0.754 ± 0.063	–	–	–

		Proposed			WMQL		
	Tracts	**WMPG**	**ISPV**	**TAPC**	**WMPG**	**ISPV**	**TAPC**
PPMI-PD	DT-45	100.0 ± 0.0	0.400 ± 0.126	0.641 ± 0.073	99.45 ± 1.04	0.501 ± 0.152	0.652 ± 0.088
	DT-13	100.0 ± 0.0	0.543 ± 0.134	0.723 ± 0.092	–	–	–
	ST-198	98.53 ± 1.39	0.656 ± 0.202	0.762 ± 0.063	–	–	–
PPMI-HC	DT-45	100.0 ± 0.0	0.423 ± 0.136	0.639 ± 0.072	99.03 ± 1.41	0.509 ± 0.140	0.652 ± 0.090
	DT-13	100.0 ± 0.0	0.524 ± 0.132	0.730 ± 0.089	–	–	–
	ST-198	98.48 ± 2.59	0.622 ± 0.171	0.762 ± 0.062	–	–	–
BTP	DT-45	95.30 ± 5.46	0.531 ± 0.126	–	–	–	–
	DT-13	96.15 ± 7.54	0.573 ± 0.104	–	–	–	–
	ST-198	93.28 ± 7.75	0.857 ± 0.220	–	–	–	–